Prospects to study a long-lived charged next lightest supersymmetric particle at the LHC

Koichi Hamaguchi

Department of Physics, University of Tokyo,
Tokyo 113-0033, Japan
E-mail: `hama@hep-th.phys.s.u-tokyo.ac.jp`

Mihoko M. Nojiri

IPNS, KEK,
Oho 1-1, 305-0801, Japan
E-mail: `nojiri@post.kek.jp`

Albert de Roeck

Physics Department, CERN,
CH-1211 Geneva 23, Switzerland, and
Universitaire Instelling Antwerpen,
B-2610 Wilrijk, Belgium
E-mail: `deroeck@mail.cern.ch`

ABSTRACT: If the scalar tau $\tilde{\tau}$ is the next lightest supersymmetric particle and decays into a gravitino($\tilde{G}$) being the lightest supersymmetric particle, it will have generally a very long lifetime. In this paper, we investigate the possibility to study the decay of such a long lived scalar tau at the LHC. If we can add to the present LHC experiments additional detectors which are able to stop the stau particles and measure the produced decay products, the decay characteristics can be studied precisely at the LHC. We identify a maximum "stopper detector" that could be added in the CMS cavern, and estimate the sensitivity to the lifetime of the stau and to the mass of gravitino with this detector. The decay of the scalar tau may be significantly modified if the decay channel to the axino $\tilde{a}$ is open. We study the possibility to distinguish such decays from decays into gravitinos by measuring the process $\tilde{\tau} \to \tilde{a}(\tilde{G})\tau\gamma$ using the stopper detector.

JHEP03(2007)046

Contents

1. Introduction

The minimal supersymmetric standard model (MSSM) is one of the most important candidates for the physics beyond the Standard Model. The strongly interacting superpartners, gluinos and squarks with mass lighter than $2.5\,\mathrm{TeV}$ can be discovered at the Large Hadron Collider at CERN (LHC) [1]. The physics run of LHC will start in 2008.

Among the supersymmetric (SUSY) particles, the lightest SUSY particle (LSP) plays a key role. In cosmology, it is a candidate for the cold dark matter in the universe. At the LHC, the signals of the supersymmetric particles depends on the nature of the LSP. It may be the lightest neutralino $\tilde{\chi}_1^0$, which escapes from detection and leads to missing E_T in the event. Another possibility for the LSP is the gravitino $\tilde{G}$, the superpartner of the graviton. The gravitino coupling to other particles in the MSSM sector is extremely small, namely proportional to $1/M_{\mathrm{pl}}$. The next lightest SUSY particle (NLSP), whose decay products necessarily include the gravitino, is therefore long-lived.

We discuss the scenario where the LSP is the gravitino and the long-lived NLSP carries charge. A natural candidate for a charged NLSP (CNLSP) is the lightest scalar tau, $\tilde{\tau}_1$,

which can be significantly lighter than the other sleptons due to the left-right mixing induced by the off diagonal matrix element $m_{LR}^2 \sim m_\tau \mu \tan\beta$. The charged particle leaves tracks in the central detectors (ATLAS and CMS), giving additional information for the SUSY particle reconstructions. If the NLSP decays in the main detectors, a displaced vertex may be observed as well.

The expected lifetime of the CNLSP $\tilde{\tau}$ is unconstrained, because it is proportional to $(m_{\tilde{G}})^2$ the yet unknown gravitino mass squared. On the other hand, the gravitino mass is proportional to the total SUSY breaking scale in the hidden sector, therefore the determination of the lifetime is an important physics goal. The lifetime measurement gives direct information on the hidden sector.

A particle decays efficiently in the main detectors (CMS and ATLAS) if the decay length is sufficiently short, $c\tau \ll (10\text{m}) \times N_{\text{produced}}$, where N_{produced} is the number of produced SUSY particles. On the other hand, for typical SUSY production cross sections, a direct observation of the decay is very difficult for $\tau_{\text{CNLSP}} > 0.01$ sec. However, it has been pointed out that the CNLSP stopped by the ionization loss in the material may be studied in detail [2, 3]. An idea for a stopper based on a water tank is presented in ref. [3], where the water can be transported away from the detector site, for concentration and further study. In ref. [2], a detector consisting of a tracker and heavy stopping material is proposed, which can measure the arrival time and the location where the CNLSPs are stopped, in addition to the energy of the decay products. Another possibility, which requires minimal experimental modification, is to study the CNLSP which are stopped in the main detector or surrounding rock [4].

As pointed out in ref. [5], the study of the CNLSP decays can probe the underlying supergravity in nature. With the gravitino mass inferred from the kinematics, the additional CNLSP lifetime measurement will test an unequivocal prediction of supergravity. Moreover, the study of a rare 3-body decay $\tilde{\tau} \to \tau \gamma \tilde{G}$ can reveal the peculiar couplings of the gravitino and the gravitino spin 3/2.

In this paper, we consider the physics of the CNLSP $\tilde{\tau}$ decays that can be done with the heavy material stopper-detector [2], because only a detector of this type can cover a wide range of lifetime $O(10\text{nsec}) < \tau_{\text{CNLSP}} < \mathcal{O}(10 \text{ years})$. We find that the mass of the gravitino can be measured if it is sufficiently heavy (roughly $m_{\tilde{G}} > 0.2 m_{\tilde{\tau}}$). In that case, one can check if the lifetime is consistent with the supergravity interpretation.

As we shall see, the LSP mass resolution is however poor if $m_{\tilde{G}} \lesssim 0.2 m_{\tilde{\tau}}$. In that case, it is very hard to prove that the decay $\tilde{\tau} \to \tau$ plus an invisible particle X is indeed caused by the supergravity interaction involving $\tilde{G}$. We should note that, because of the extremely weak coupling of the gravitino, if there is any unknown supersymmetric particle X which couples rather weakly to the MSSM particles, the lightest MSSM particle may decay into X instead of $\tilde{G}$ even if the $\tilde{G}$ is the LSP. For example, the superpartner of the axion, the axino $\tilde{a}$, can be such a particle. However, we found that it may be possible to discriminate the case of $X = \tilde{G}$ and the case of $X = \tilde{a}$, by investigating the three body decay $\tilde{\tau} \to \tau \gamma X$ as suggested in [5, 6], with enough statistics.

This paper is organized as follows. In section 2, we discuss a possible detector setup. We found an $\mathcal{O}(1)$ kton detector (up to 8 kton) may be placed next to the CMS detector

	diameter	weight of the detector	length
ATLAS	22m	7Kt	44m
CMS	15m	12.5Kt	21m

without serious modification of the CMS experiment itself, but with non-negligible modifications to the CMS cavern side walls. In section 3, we select several model points and estimate the expected number of the stopped particles for $\int \mathcal{L} = 300$ fb^{-1} and $3000\,$fb^{-1}. In section 4, we discuss the measurement of the two body decay $\tilde{\tau} \to \tau X$. The three body decay of the CNLSP is studied in section 5. Section 6 contains the discussion and comments.

2. Assumptions on the stoppers

In this section, we discuss the possibility to install massive stoppers next to the LHC detectors, CMS and ATLAS. It turns out that the CMS cavern may allow for an easier installation and more room for a massive stopper, compared to the ATLAS cavern. The parameters of the two detectors are listed in table 2. The diameter of the CMS detector is smaller, therefore the massive stopper can be placed closer to the interaction point at CMS. The weight of the CMS detector is about twice as large as that of ATLAS. Because of the large weight, the cavern of CMS is designed so that it can sustain a massive object safely, which includes a reinforced floor to spread the detector pressure more equally. A potential massive stopper with a weight of around a few kton can be placed on both sides of the CMS detector, but it will need a reorganization of the scaffolding and gallery paths on the cavern walls, to make room for such an additional detector.

The assembly and construction of the two detectors is also very different. Most of the CMS detector components are assembled on the ground, and about 15 large detector units will be lowered in the cavern for final assembly works. Hence the installation is less integrated with the cavern, leaving relatively more freedom and thus changes needed in the cavern to install massive stoppers are somewhat simpler [7]. On the other hand ATLAS detector is assembled mostly in its cavern. The huge magnets toroids and outside muon system fill up the cavern. The cryogenic system in the ATLAS cavern is also taking space outside the detector [8].

We assume two stoppers with the size 3.5m × 15m × 15m and the average density $\rho_{\text{stop}} = 5\text{g/cm}^3$, hence, the total weight of the detector is 8 kton. This is maximum possible rectangular parallelepiped volume that can be placed in the cavern, with the given space to the cavern wall and with its long edge being the same as that of the CMS barrel part (see figure 1). The stoppers are thus placed 8.5 m away from the interaction point. We also assume that stopping power of the CMS detector is equivalent to $(2500/\sin\theta)$ g/cm^2 iron, where θ is angle between the CNLSP direction and the beam direction. The number comes from the average density of CMS detector, 3.37g/cm^3, which leads to the weight per cm^2 for the radial direction of 2500g/cm^2.
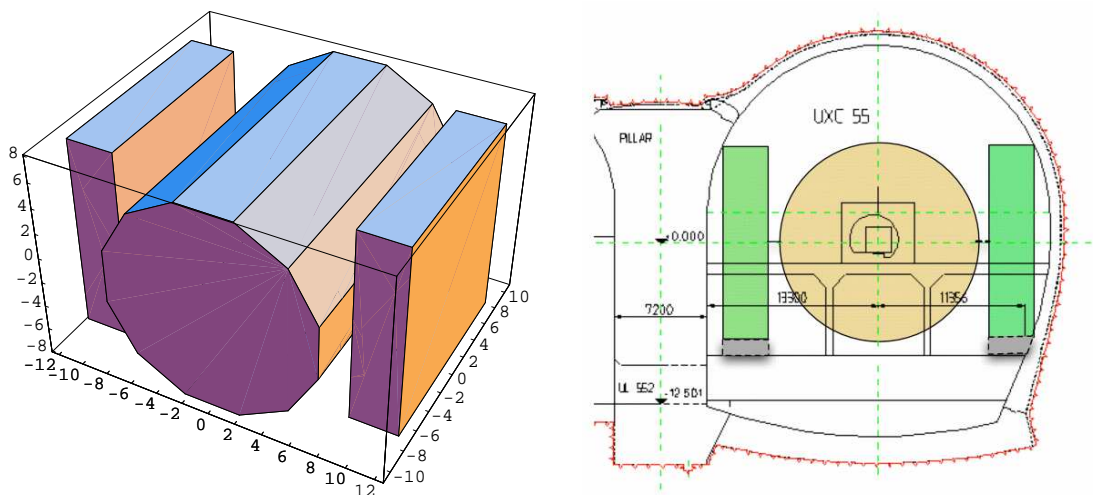
Figure 1: Left: a schematic figure of the CMS detector and two stoppers. The numbers are in units of meters, and $(0, 0, 0)$ is the collision point. Right: two stopper-detectors and a circle about the size of CMS detector are superimposed on the cross section of CMS cavern UXC 55, drawing taken from ref. [9].

As discussed in the previous paper [2], the stopper can be a hadronic and electromagnetic calorimeter simultaneously, if the detector consists of layers of dense stopper and tracking devices. The measurement of the energy of the decay product of the CNLSP is the key ingredient to explore the CNLSP interactions to the X particle. In this paper we assume that the CNLSP is the scalar tau lepton $\tilde{\tau}$, which decays mostly as $\tilde{\tau} \to \tau X$ where $X = \tilde{G}$ or $\tilde{a}$.

The τ decays into $l\bar{\nu}_l\nu_\tau$, or into $\pi^\pm$ and π^0's. We do not consider the decays into μ, because the muon energy cannot be measured unless the stopper contains a magnetic field. The energy of the leptons are much softer than the parent τ energy anyway, so that they are less useful for the study of the decay kinematics.

A large volume detector is advantageous to measure the energy of the τ decay products, because the detector must contain most of the energy of the showers from the τ decay products. To fully absorb the hadronic cascade one needs sufficient thickness of the calorimeter. The required thickness for an iron calorimeter (density is $7.87\mathrm{g/cm^3}$) is listed in ref. [10, 11], and is about 170 (120) cm for $100\,\mathrm{GeV}$ single hadron energy for 99% (95%) containment respectively, equivalent to $1337.9\mathrm{g/cm^2}$ ($944.4\mathrm{g/cm^2}$). To measure the energy with sufficient accuracy by a stopper with $\rho = 5\mathrm{g/cm^3}$, the distance between the decay position and the end of the detector along the shower path must be at least 190cm. A simplified Monte Carlo simulation shows that 63% of the $\tilde{\tau}$ decays satisfy this condition. High energy photons and electrons initiate electromagnetic cascades, which are much easier to contain in a detector. The energy deposition along the axis of the cascade is well described by a gamma distribution, where the maximum occurs at $\sim 8X_0$, where X_0 is the radiation length. The energy deposition terminates around $15X_0$. (See figure27.17 of [10].) For the

case of iron ($X_0 = 13.84\text{g/cm}^2$), 200g/cm² thickness of the material is needed to stop the electromagnetic cascade. The difference in the absorption length is used to discriminate isolated photons from hadron, which would be useful to study $\tilde{\tau} \to \tau \gamma X$ decay.

In a previous paper [2], we discussed the possibility to re-use of the existing 1 kton detector, such as SOUDAN II [12] as the CNLSP stopper. The SOUDAN II consists of the layers of $\mathcal{O}(\text{m})$ long drift tubes and thin iron plates. The physics goal of this detector is the search for proton decays. To be sensitive to the low energies involved in these decay processes, the average density of SOUDAN II is low, less than 2g/cm³. The size of the detector is probably enough to stop a certain amount of CNLSPs and measure the decay rate, and therefore it may well be appropriate for the a first stage of the CNLSP study. On the other hand, it is certainly not enough for a detailed energy measurement of the $\tilde{\tau}$ decay product. Most of the hadronic decay cascades are not fully contained for a detector with the geometry allowed by the space in the CMS cavern. A high density detector consisting of the layers of drift tubes/scintillators or RPCs to measure the charged particles between iron plates thicker than SOUDAN II will be more optimized for the CNLSP study.

In this paper we assume a conservative energy resolution for hadronic showers, which is around $150\%/\sqrt{E/\text{GeV}}$. The value is not unrealistic for a simple massive and affordable detector, if a shower is sufficiently contained in the stopper. An additional complexity may occur for showers which develop parallel to the layers of the tracking devices. If the particles pass mostly through tracking devices, they feel a much lower average density, while the particles going mostly through the iron plates do not give detectable signature efficiently. We assume that the measured energy will be corrected depending on the shower directions. A detector uniform to all directions would be better to measure the energy of decay products of the stopped CNLSP. The calorimetery technologies studied for the ILC may satisfy such conditions; see [13] for the CNLSP study at ILC.

3. Supersymmetric models with charged next lightest SUSY particles, and expected number of stopped CNLSP

In this section, we briefly describe supersymmetric models with a long-lived charged next lightest SUSY particle. We also select some model points, and estimate at each model point the number of CNLSP that can be stopped at the stopper-detector.

In the minimal supergravity (mSUGRA) models, the scalar masses and gaugino masses, trilinear couplings are universal at the GUT scale M_{GUT} which are denoted by m_0, $M_{1/2}$, and A_0 respectively. The resulting mass spectrum is obtained by solving renormalization group equations (RGE's). When the RGE is integrated up to $\mathcal{O}(m_Z)$, slepton soft masses and gaugino masses are approximately given by the following convenient formulas

$$
\begin{aligned}
m_{\tilde{q}_L}^2 &\sim m_0^2 + 6.3 M_{1/2}^2, & m_{\tilde{u}_R}^2 \simeq m_{\tilde{d}_R}^2 &\sim m_0^2 + 5.4 M_{1/2}^2, \\
m_{\tilde{\ell}_L}^2 &\sim m_0^2 + 0.5 M_{1/2}^2, & m_{\tilde{e}_R}^2 &\sim m_0^2 + 0.15 M_{1/2}^2, \\
\frac{M_i}{g_i^2} &= \frac{M_{1/2}}{g_X^2},
\end{aligned}
\tag{3.1}
$$

where g_X is the gauge couplings at the unification scale.[1] In this model, the mass of gravitino $m_{\tilde{G}}$ is order of m_0 or $M_{1/2}$, because both of them are proportional to the $F_0/M_{\rm pl}$ with $\mathcal{O}(1)$ coefficient, where F_0 is the fundamental SUSY breaking scale. Depending on the $\mathcal{O}(1)$ coefficients, the gravitino can be the lightest superparticle in general. Also in the gaugino mediation models [14], the gravitino can be the LSP in a large domain of the parameter space [15]. In this case the scalar masses are very small at the boundary, i.e., $m_0 \simeq 0$, and the stau naturally becomes the NLSP.

In the gauge mediation (GM) model [16] the supersymmetry is broken at lower energy scale, and the SUSY breaking in the hidden sector is mediated to the MSSM sector by gauge interactions. The simplest GM model is described by 6 parameters: $\Lambda = F/M_{\rm mes}$, $M_{\rm mes}$, N_5, $\tan\beta$, sgn$\mu = \pm 1$ and gravitino mass. Here N_5 is an effective number of vector-like heavy quarks and leptons in SU(5) representations, Φ and $\bar{\Phi}$. ($N_5 = 1$ for $5 + \bar{5}$ quarks and leptons, and $N_5 = 3$ for $10 + \overline{10}$.) A messenger field Y couples to the vector-like fields as $W = \lambda Y \Phi \bar{\Phi}$ and develops a vacuum expectation value $\lambda\langle Y \rangle = M_{\rm mes} + \theta\theta F$. The gravitino mass is given by $m_{\tilde{G}} = F_0/(\sqrt{3}M_{\rm pl})$ where $F_0 (\geq F)$ is the total SUSY breaking scale of the theory. We take $m_{\tilde{G}}$ as a free parameter in this model.

The masses of MSSM particles at $M_{\rm mes}$ are obtained by relatively simple formula. Gaugino masses satisfy the GUT relation, and

$$m_{\tilde{g}} = \frac{\alpha_s}{4\pi} N_5 \Lambda. \tag{3.2}$$

Squark and slepton masses are given by

$$
\begin{aligned}
m_{\tilde{q}_L}^2 &= \left[\frac{8}{3}\left(\frac{\alpha_s}{4\pi}\right)^2 + \frac{3}{2}\left(\frac{\alpha_2}{4\pi}\right)^2 + \frac{1}{30}\left(\frac{\alpha_1}{4\pi}\right)^2 \right] N_5 \Lambda^2, \\
m_{\tilde{u}_R}^2 &= \left[\frac{8}{3}\left(\frac{\alpha_s}{4\pi}\right)^2 + \frac{8}{15}\left(\frac{\alpha_1}{4\pi}\right)^2 \right] N_5 \Lambda^2, \\
m_{\tilde{d}_R}^2 &= \left[\frac{8}{3}\left(\frac{\alpha_s}{4\pi}\right)^2 + \frac{2}{15}\left(\frac{\alpha_1}{4\pi}\right)^2 \right] N_5 \Lambda^2, \\
m_{\tilde{\ell}_L}^2 &= \left[\frac{3}{2}\left(\frac{\alpha_2}{4\pi}\right)^2 + \frac{3}{10}\left(\frac{\alpha_1}{4\pi}\right)^2 \right] N_5 \Lambda^2, \\
m_{\tilde{e}_R}^2 &= \left[\frac{6}{5}\left(\frac{\alpha_1}{4\pi}\right)^2 \right] N_5 \Lambda^2.
\end{aligned}
\tag{3.3}
$$

All of the above models predict a large mass hierarchy between strongly interacting superpartners and weakly interacting superpartners. Heavy gluino and squarks are copiously produced at the LHC, and they decay into the light weakly interacting SUSY particles. The lightest SUSY particle in the MSSM sector is either the lighter stau $\tilde{\tau}_1$ or the lightest neutralino $\tilde{\chi}_1^0$.

The mass of the $\tilde{\tau}_1$ is the smaller eigenvalue of the mass matrix,

$$
\mathcal{M}^2 = \begin{pmatrix} m_{\tilde{\ell}_{L_3}}^2 + m_\tau^2 - \frac{1}{2}(2m_W^2 - m_Z^2)\cos 2\beta & -m_\tau(A_\tau + \mu\tan\beta) \\ -m_\tau(A_\tau + \mu\tan\beta) & m_{\tilde{\tau}_R}^2 + m_\tau^2 + (m_W^2 - m_Z^2)\cos 2\beta \end{pmatrix}. \tag{3.4}
$$

---

[1]The pole masses of strongly interacting SUSY particles receive a large corrections of $\mathcal{O}(30\%)$ if the mass scale is $\mathcal{O}(1\text{TeV})$.

Point	ϵ	ζ	η
$M_{1/2}$	440	1000	1000
m_0	20	100	20
$\tan\beta$	15	21.5	23.7
$m_{\tilde{g}}$[GeV]	1025	2191	2190
$m_{\tilde{\chi}_1^0}$[GeV]	175	417	416
$m_{\tilde{\tau}_1}$[GeV]	154.2	343.5	324.3
σ(SUSY)[pb]	3.03	2.27×10^{-2}	2.34×10^{-2}
stopped in the stopper-detector per 10^5 events	255	250	254
stopped for $300\,\mathrm{fb}^{-1}$	4636	34	36

Table 1: Some model points in mSUGRA model from [4]. The mass spectrum and production cross section relevant to our study are shown.

Λ[TeV]	40	50	60	70	80
$m_{\tilde{g}}$[TeV]	0.93	1.13	1.34	1.54	1.74
$m_{\tilde{\chi}_1^0}$[GeV]	161.7	205.3	248.7	292.1	335.4
$m_{\tilde{\tau}_1}$[GeV]	120.5	150.1	179.9	209.8	239.9
σ(SUSY)[pb]	5.24	1.68	0.64	0.28	0.13
stopped in the stopper-detector per 10^5 events	282	274	274	294	302
stopped for $300\mathrm{fb}^{-1}$	8830	2762	1052	494	236

Table 2: Some model points in gauge mediation model. The production cross section and mass spectrum relevant in this study are also shown.

Because of the off-diagonal elements of $\tilde{\tau}$ mass matrix, $\tilde{\tau}_1$ could be significantly lighter than the other sleptons. If the $\tilde{\tau}_1$ is the NLSP, the stopper-detector is useful to stop it and to study its decay. We therefore consider the phenomenology when $m_{\tilde{g}}, m_{\tilde{q}} \gg m_{\tilde{\chi}_1^0} > m_{\tilde{\tau}_1}$ in this paper. In the following, we omit the subscript of $\tilde{\tau}_1$ and denote the NLSP stau as $\tilde{\tau}$.

In most part of this paper, we will discuss the CNLSP physics as model independent as possible. However, to give some numerical reference, we choose a few model points. For mSUGRA models, we take the points proposed in [4]. The parameters are listed in table 1 and mass spectrum is given by the ISAJET ver. 7.69. In [4], the gravitino mass is taken to be $m_{\tilde{G}} = m_0$ in those model points.

For the gauge mediation model, we take the model points similar to that for the study in [1]. Namely, we fix $N_5 = 3$, $\tan\beta = 15$ and $\Lambda/M_{\mathrm{mes}} = 0.5$, where $\Lambda = 40, 50, 60, 70, 80$ TeV. The mass spectrum and production cross sections are summarized in table 2. The gravitino mass for these models can be very small, whose minimum value is given by $\mathcal{O}(\Lambda^2)/M_{\mathrm{pl}}$. If the messenger sector couples a fraction of total SUSY breaking, i.e. $F < F_0$, the gravitino mass, which is proportional total SUSY breaking F_0, can be large.

The pattern of the mass spectra are similar for both mSUGRA and GM sample points. The gaugino masses obey the GUT relation, and $\tilde{\tau}$ mass is lighter than $\tilde{B}$ mass because of

the CNLSP assumption. For mSUGRA, this implies $m_0 < M_{1/2}$, so that $\tilde{q}$ mass is about as large as $\tilde{g}$, as it is so in GM models. The relation $m_{\tilde{q}} \sim m_{\tilde{g}} \gg m_{\tilde{\tau}}$ is realized in our model points.

To estimate the number of stopped CNLSP, the production cross section of the SUSY particles and the velocity distribution of $\tilde{\tau}$ at LHC must be evaluated. They depend on the $\tilde{g}$ and $\tilde{q}$ masses, and the mass difference $m_{\tilde{g}(\tilde{q})} - m_{\tilde{\tau}}$. We estimate the production cross section and the decay distribution by using HERWIG [17], where the mass spectrum and branching ratios are interfaced from ISAJET [18] to HERWIG by using ISAWIG [19]. We generated 10^5 SUSY events for each model point.

The flying range R of the charged stable massive particle may be calculated by integrating the energy loss equation of heavy ionizing particle (Bethe-Bloch equation). The result is a function of $\beta = p/E$, with a linear dependence on the mass of the particle M. In this paper, the stopping power of the stopper-detector is calculated using the data in [20]. See also the detailed discussion in ref. [3].

The maximum length of a particle track through the stopper-detector $l(\max)$, which depends on CNLSP direction, is calculated assuming that the track of the CNLSP goes straight from the production point. We regard the particle is stopped in the stopper-detector if the flying range R satisfies:

$$\frac{2500 \text{ g/cm}^2}{\sin\theta} \; < \; R \; < \; \frac{2500 \text{ g/cm}^2}{\sin\theta} + l(\max) \times \rho_{\text{stop}} \,, \tag{3.5}$$

where $\rho_{\text{stop}} = 5\text{g/cm}^3$ is the density of the stopper-detector. The number of stopped CNLSP in a stopper per 10^5 events, and the number of stopped CNLSP for $\mathcal{L} = 300\text{fb}^{-1}$ in the two stoppers, are listed in table 1 and 2. In figure 2 we also show the simulated stopped positions in a stopper-detector. The position distribution is uniform in the detector.

In figure 3, we show the $\beta\gamma$ distribution of the CNLSPs for a few model points. We find that CNLSP tends to be less relativistic when the SUSY scale is large, because momentum of parent squarks and gluino is reduced. In figure 3, the peak position of the $\beta\gamma$ is at $\sim 1.5(1.3)$ for $\Lambda = 50(80)\,\text{TeV}$. Because of that, the number of CNLSP in the smaller $\beta\gamma$ region is increased as the SUSY scale is increased. On the other hand, as m_{CNSLP} increases, CNLSPs with smaller $\beta\gamma$ are stopped in the detector while the number of events in the smaller $\beta\gamma$ bins are kinetically suppressed. For instance, for $\Lambda = 50$ and $80\,\text{TeV}$, CNLSPs in the bins between $0.5 < \beta\gamma < 0.6$ and $0.45 < \beta\gamma < 0.55$ are stopped in the stopper-detector, respectively. Altogether, the number of stopped $\tilde{\tau}$ for $\Lambda = 40$ to $80\,\text{TeV}$ for 10^5 SUSY events is roughly constant as we can see in table 2.

The production cross section reduces when the gluino mass is increased because the parton distribution functions of gluon and quarks are quite small for $x \gg 0.1$. For 300fb^{-1}, the number of events stopped at the assumed two 4 kton stoppers ranges from 8000 events to 30 events in the table. We will see in the next section that accumulation of $\mathcal{O}(100)$ CNLSPs are enough to measure the lifetime with $\mathcal{O}(10)\%$ accuracy. We will also estimate the resolution of τ lepton energy E_τ arising from the decay $\tilde{\tau} \to \tau X$ through the end point of the tau jet energy. Statistically $\mathcal{O}(1000)$ stopped CNLSPs are enough to measure the end point with a few GeV error. In the upgrade of LHC (SLHC), integrated luminosity
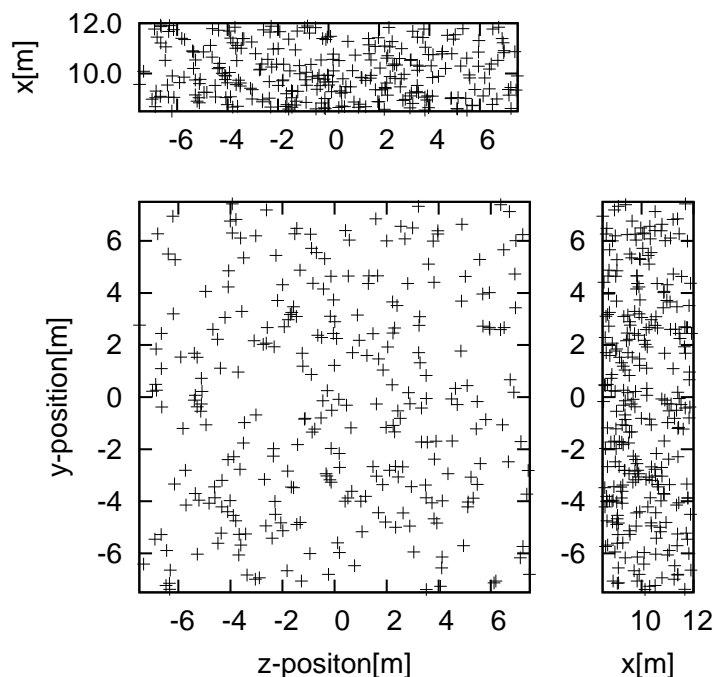
Figure 2: The simulated positions of the CNLSPs in a stopper-detector for the $\Lambda = 40\,\mathrm{TeV}$ GM point. Here the z axis is the beam direction, and the y axis is the vertical direction. The origin $(0,0,0)$ is the interaction point and we assume the stopper-detector is at $8.5\mathrm{m} < x < 12\mathrm{m}$, $-7.5\mathrm{m} < y < 7.5\mathrm{m}$, and $-7.5\mathrm{m} < z < 7.5\mathrm{m}$ (cf. figure 1). The big square is the projection on the y-z plane, the top rectangle is the projection on the x-z plane, and the right rectangle is the projection on the x-y plane.

of $3000\mathrm{fb}^{-1}$ is proposed, therefore the number of stopped events ranges from $\mathcal{O}(300)$ to $\mathcal{O}(80000)$ for the model points presented in table 2.

4. Study of the $\tilde\tau$ two body decay in stopper-detector

In this section we study the two body decay of the CNLSP in the stopper-detector. Both in mSUGRA and GM models, the stau can be the CNLSP and decays into the gravitino $\tilde{G}$ and the τ-lepton. The CNLSP decay width into a gravitino and a lepton is given by [5]

$$
\begin{aligned}
\Gamma_{\tilde\tau}(\tilde\tau \to \tilde{G}\tau) &= \frac{m_{\tilde\tau}^5}{48\pi m_{\tilde{G}}^2 M_{\mathrm{pl}}^2} \left(1 - \frac{m_{\tilde{G}}^2 + m_\tau^2}{m_{\tilde\tau}^2}\right)^4 \left[1 - \frac{4m_{\tilde{G}}^2 m_\tau^2}{(m_{\tilde\tau}^2 - m_{\tilde{G}}^2 - m_\tau^2)^2}\right]^{3/2}. \\
&= (68\ \mathrm{days})^{-1} \left(\frac{m_{\tilde\tau}}{100\ \mathrm{GeV}}\right)^5 \left(\frac{10\ \mathrm{GeV}}{m_{\tilde{G}}}\right)^2 \times \\
&\quad \left(1 - \frac{m_{\tilde{G}}^2 + m_\tau^2}{m_{\tilde\tau}^2}\right)^4 \left[1 - \frac{4m_{\tilde{G}}^2 m_\tau^2}{(m_{\tilde\tau}^2 - m_{\tilde{G}}^2 - m_\tau^2)^2}\right]^{3/2}.
\end{aligned} \tag{4.1}
$$

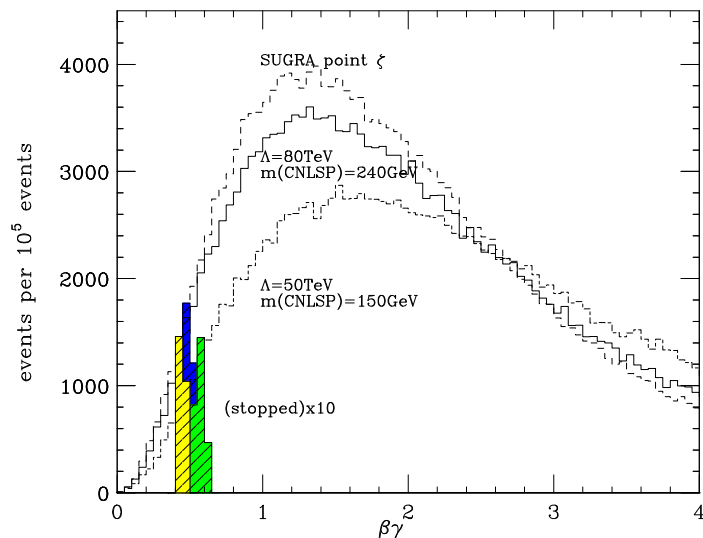We show the dependence of the stau lifetime on the gravitino mass in figure 4.

Figure 3: The $\beta\gamma$ distribution of $\tilde{\tau}$ for $\Lambda = 80$ TeV and $\Lambda = 50$ TeV in GM models and for point ζ in mSUGRA models for 10^5 SUSY events. Light (dark, gray) shaded histograms are the number of stopped events in the stopper scaled by factor of 10, for point ζ and for GM models with $\Lambda = 80, 50$ TeV respectively.
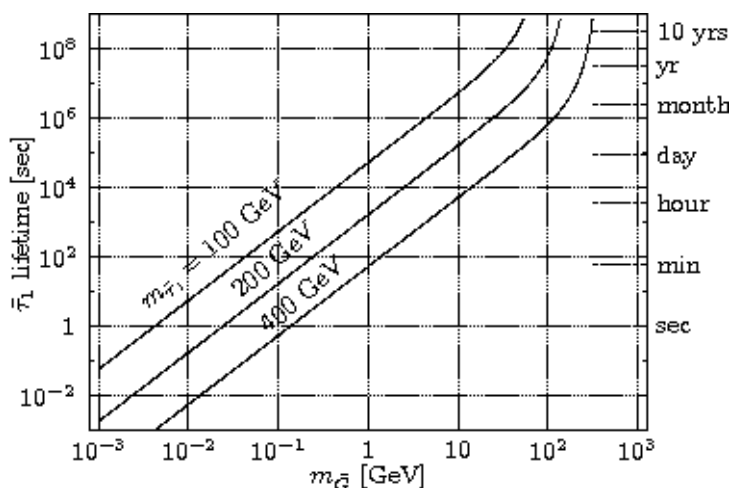

Figure 4: The lifetime of the CNLSP $\tilde{\tau}$ in the case of gravitino LSP, as a function of the gravitino mass, for the stau mass 100, 200, and 400 GeV (from top to bottom).

In general, the two-body decay $\tilde{\tau} \to X\tau$ can be triggered by a single tau jets initiating from the position where $\tilde{\tau}$ is stopped. The tau energy is monochromatic and expressed as

$$E_\tau = \frac{m_{\tilde{\tau}}^2 + m_\tau^2 - m_X^2}{2m_{\tilde{\tau}}} . \tag{4.2}$$

Here X is the invisible particle in the $\tilde{\tau}$ decay, in this case $X = \tilde{G}$. If one can measure both of the lifetime and the mass of the stau, the gravitino mass can be determined *assuming*
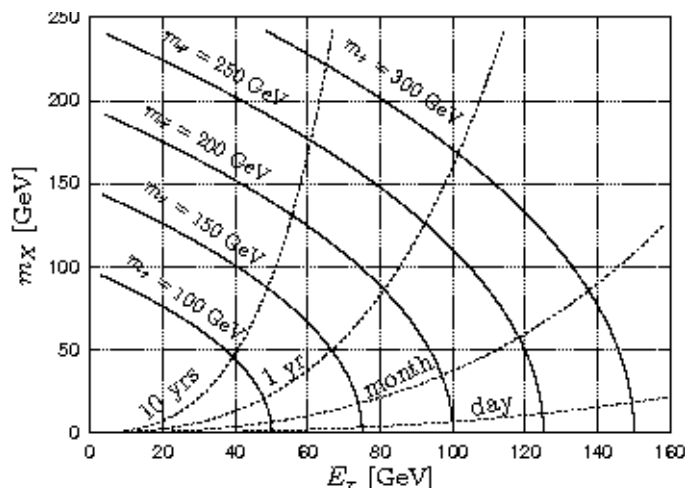
Figure 5: Sensitivity of the reconstructed LSP mass m_X [see eq. (4.3)] on the tau energy E_τ, for $m_{\tilde\tau} = 100$, 150, 200, 250, and $300\,\mathrm{GeV}$ (solid lines). Dashed lines show contours of the lifetime in the case of the gravitino LSP ($X = \tilde{G}$).

that eq. (4.1) is correct. Then the total SUSY breaking scale $F_0 = \sqrt{3}m_{\tilde{G}}M_{\rm pl}$ is also determined, which is very important to understand the hidden sector physics.

The LHC main detectors can determine the mass of $\tilde\tau$ through the stau velocity measurement $\beta_{\tilde\tau}$, e.g., in the muon system of the CMS detector. However, the measurement of the lifetime may not be easy at the main detectors if the lifetime is too much longer than the detector size. The cross section is typically $\mathcal{O}(1)$ pb or less, therefore we have at most $\mathcal{O}(10^5)$ event at hand for $\mathcal{L} = 100\,\mathrm{fb}^{-1}$. Thus, only 10 events or less decay inside the detector if $c\tau > 100$ km. Some of the CNLSP are stopped in the main detector, but measuring the decay precisely in the main detector would be challenging during the beam time. On the other hand a stopper-detector [2] can measure the position and the time where a CNLSP is stopped, and its decays without dead-time. The lifetime measurement will be discussed in section 4.1. See [4] also on the idea to measure the lifetime by triggering muons from the decays of the CNLSP stopped in the surrounding rock.

To *predict* the CNLSP lifetime, one has to determine the gravitino mass independently. This is possible through the extraction of E_τ from the energy distribution of the tau jet from the CNLSP decay, because E_τ is a function of $m_{\tilde\tau}$ and m_X, as can be seen in eq. (4.2). m_X is expressed as a function of E_τ as follows;

$$m_X = \sqrt{m_{\tilde\tau}^2 + m_{\tilde\tau}^2 - 2m_{\tilde\tau}E_\tau}\,. \tag{4.3}$$

Figure 5 shows the dependence of the reconstructed LSP mass eq. (4.3) on the tau energy E_τ for several values of $m_{\tilde\tau}$. As can be seen from the figure, it is crucial to measure the E_τ as precise as possible, especially for small m_X, in order to determine the mass m_X. Hence, the stopper-detector should offer a reliable measurement of E_τ. We will discuss the E_τ measurement and the m_X reconstruction in section 4.2 and section 4.3, respectively.

One can study the supersymmetric version of gravity interaction by studying the consistency between the observation and prediction of the decay rate. If the gravitino is the LSP, the decay width is given by eq. (4.1). Now if one can independently determine the gravitino mass by means of kinematics, as described above, eq. (4.1) can be used in the other way round, which leads to the measurement of the 'supergravity Planck scale' [5]

$$M_{\rm pl}^2({\rm supergravity}) = \frac{m_{\tilde\tau}^5}{48\pi m_{\tilde G}^2 \Gamma_{\tilde\tau}} \left(1 - \frac{m_{\tilde G}^2 + m_\tau^2}{m_{\tilde\tau}^2}\right)^4 \left[1 - \frac{4m_{\tilde G}^2 m_\tau^2}{(m_{\tilde\tau}^2 - m_{\tilde G}^2 - m_\tau^2)^2}\right]^{3/2}. \quad (4.4)$$

Comparison of the obtained $M_{\rm pl}({\rm supergravity})$ with the Planck scale of the Einstein gravity $M_{\rm pl}({\rm gravity}) = (8\pi G)^{-1/2} = 2.43534(18) \times 10^{18}$ GeV [10] would be a crucial test of the supergravity. Prospects of the "Planck scale" measurement will be discussed in section 4.4.

It should be noted that the undetectable particle X may not be the gravitino $\tilde G$. Any particle which couples weakly to $\tilde\tau$ can be particle X. If the decay width into $X\tau$ is larger than the decay width into $\tilde G\tau$, i.e. $\Gamma(\tilde\tau \to \tau X) > \Gamma(\tilde\tau \to \tau\tilde G)$,[2] the CNLSP lifetime may be different from the supergravity prediction obtained from measured $m_{\tilde\tau}$ and tau jet energy distribution. Inconsistency between the measured and predicted lifetime immediately means a discovery of a new sector that may not be accessible otherwise.

One of well motivated examples of such a non-SUGRA decay is $\tilde\tau \to \tilde a\tau$ where $\tilde a$ is the axino, superpartner of the axion. The CNLSP $\tilde\tau$ decay into axino is studied in ref. [6] for hadronic, or KSVZ axion models [21]. In this paper we adopt the set-up in ref. [6] for the axino interaction, which we briefly describe here.

In KSVZ axion model, the Peccei-Quinn (PQ) mechanism [22] is realized in an action with new heavy quarks. When these heavy quarks are integrated out, anomalous terms involving the axion and gauge bosons are generated at low energy effective action. When the axion interaction is supersymmetrized, its fermionic superpartner, the axino $\tilde a$, must be introduced. The axino mass $m_{\tilde a}$ can range between the eV and GeV scale depending on the model and SUSY breaking scheme [23], and we regard it as a free parameter in this paper. The coupling of the axino to the bino and the photon/Z-boson at the scale below the Peccei-Quinn scale f_a is given by the Lagrangian

$$L_{\tilde a} = i\frac{\alpha C_{aYY}}{16\pi \cos^2\theta_W f_a}\bar{\tilde a}\gamma_5[\gamma_\mu, \gamma_\nu]\tilde B(\cos\theta_W F_{\mu\nu} - \sin\theta_W Z_{\mu\nu}). \quad (4.5)$$

The action does not contain direct $\tilde\tau\tau\tilde a$ coupling and also strongly suppressed by the PQ scale $10^9{\rm GeV} \lesssim f_a \lesssim 10^{11}{\rm GeV}$. The two body decay $\tilde\tau \to \tilde a\tau$ is induced by the one loop diagram shown in figure 6. The loop integral has a logarithmic divergence. This is because the effective vertex (4.5) is applicable only if the momentum is smaller than the heavy (s)quark masses, whereas the loop momentum exceeds that scale. In the full theory, one calculates two-loop diagrams with the heavy (s)quarks, which leads to a finite result [24]. Here we regulate the logarithmic divergence with the cut-off $\sim f_a$ [6, 25], and the effective

---

[2]This includes the trivial case where the decay into the gravitino is kinetically forbidden, $\Gamma(\tilde\tau \to \tau\tilde G) = 0$, i.e., $m_{\tilde G} > m_{\tilde\tau} > m_X$.
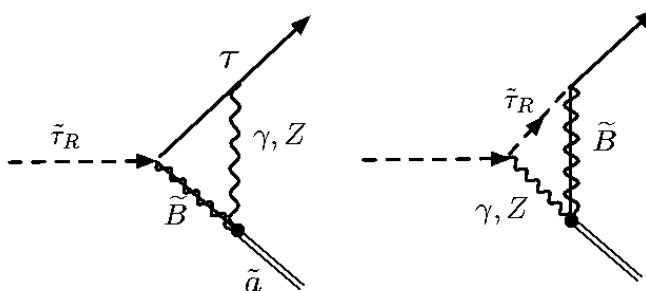
Figure 6: Feynman diagrams for $\tilde{\tau} \to \tilde{a}\tau$.

$\tilde{a}\tau\tilde{\tau}_R$ coupling is parameterized as

$$L \simeq -\xi C_{aYY} \frac{3\sqrt{2}\alpha^2}{8\pi^2 \cos^4 \theta_W} \frac{m_{\tilde{B}}}{f_a} \log \frac{f_a}{m} \tilde{\tau}_R \bar{\tau} P_L \tilde{a} + hc, \tag{4.6}$$

Here, $m \simeq m_{\tilde{\tau},\tilde{B}} \simeq \mathcal{O}(100 \text{ GeV})$ and we take $\log(f_a/m) = 20.7$ hereafter. The parameter ξ is an order one parameter to represent the uncertainty coming from the cut-off procedure mentioned above. In this paper, we regard this as a free parameter. The two body decay width is given as [6]

$$\Gamma(\tilde{\tau} \to \tilde{a}\tau) = \frac{9\alpha^4 C_{aYY}^2}{512\pi^5 \cos^8 \theta_W} \frac{m_{\tilde{B}}^2}{f_a^2} \frac{(m_{\tilde{\tau}}^2 - m_{\tilde{a}}^2)^2}{m_{\tilde{\tau}}^3} \xi^2 \log^2 \left(\frac{f_a}{m} \right) \tag{4.7}$$

$$= \xi^2 (25 \text{ sec})^{-1} C_{aYY}^2 \left(1 - \frac{m_{\tilde{a}}^2}{m_{\tilde{\tau}}^2} \right)^2 \left(\frac{m_{\tilde{\tau}}}{100 \text{GeV}} \right) \left(\frac{10^{11} \text{GeV}}{f_a} \right)^2 \left(\frac{m_{\tilde{B}}}{100 \text{GeV}} \right)^2.$$

4.1 Lifetime measurement

In this subsection, we estimate the statistical error in the CNLSP lifetime measured by the stopper-detector. The analysis is model-independent and applicable to any long-lived charged particle stopped in the stopper.

For each CNLSP stopped in the stopper-detector, the stopping time t_{stop} and the decaying time t_{decay} will be recorded. The lifetime is then measured by fitting the temporal distribution of the decaying events $N(t)$, where $t = t_{\text{decay}} - t_{\text{stop}}$. Here, we use a maximum-likelihood fitting and adopt the following procedure: First we define a time t_e such that $N(t < t_e) = (1 - e^{-1})N_{\text{total}} \simeq 0.632 N_{\text{total}}$ and $N(t > t_e) = e^{-1} N_{\text{total}} \simeq 0.368 N_{\text{total}}$, where N_{total} is total number of stopped event.[3] (For large N_{total}, this t_e is already a good estimator of the lifetime.) We then calculate the $\ln L$ distribution as a function of lifetime τ:

$$\ln L(\tau) = \sum_{i=\text{bins}} f_{\text{P}}(n_i; \nu_i(\tau)) \tag{4.8}$$

---

[3]More precisely, t_e is defined by $t_e = (t_j + t_{j+1})/2$, where $j < (1 - e^{-1})N_{\text{total}} < j + 1$ and t_j is the decay time of the j-th event: $t_1 < t_2 < \cdots < t_j < \cdots < t_{N_{\text{total}}}$.
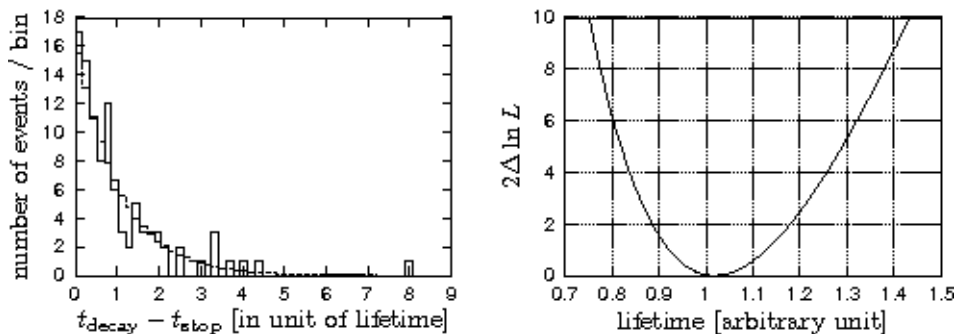
Figure 7: An example of maximum-likelihood fit of the temporal distribution $N(t)$ for $N_{\text{total}} = 100$. In the left plot, the solid line is the generated events, and dashed line is the best fit.

where $f_P(n; \nu) = \nu^n e^{-\nu}/n!$ is the Poisson distribution, n_i is the number of events in the i-th bin, and $\nu_i(\tau)$ is the predicted average number of events in that bin:

$$\nu_i(\tau) = N_{\text{total}} \left(e^{-(i-1)\Delta t/\tau} - e^{-i\Delta t/\tau} \right). \tag{4.9}$$

Here, we take 1 bin $= \Delta t = t_e/5$.

An example of the time distribution and the best fit curve for MC distribution are shown in figure 7 for $N_{\text{total}} = 100$. The $n\sigma$ confidence interval can be estimated by the range $2\Delta \ln L = 2(\ln L_{\max} - \ln L) \le n^2$. Figure 7 shows that the error of the lifetime is $\Delta\tau/\tau = (10 - 15)\%$ for $N_{\text{total}} = 100$. We have done the same analysis for $N_{\text{total}} = 1000$ and found $\Delta\tau/\tau = (3 - 4)\%$.

So far, we assumed that most of the stopped CNLSPs decay within the experimental time scale. We now consider the case where the lifetime is longer. Suppose that one observes $N_{\text{total}} = 1000$ stopped CNLSPs and only 10 events decaying within 1 year. In such a case, the lifetime is estimated from the number of the decaying events. For instance, 95% interval of the mean ν of Poisson variable for $n = 10$ is $\nu = [5.4, 17.0]$ [10]. Using $\nu = N_{\text{total}}(1 - e^{-1 \text{ year}/\tau})$, a 95% interval $58 < \tau < 184$ years is obtained. For much longer lifetime or smaller N_{total}, only a lower bound of the lifetime is obtained.

We have assumed that the background is negligible. The background from cosmic neutrino and hard neutrino produced from the main detector interaction point is small (cf. [2]), however careful study on the accidental background is necessary when statistics is low. This is beyond of the scope of this paper.

4.2 Measurement of the τ energy from distribution of the τ jet energies

In this subsection, we estimate the uncertainty of the tau energy determination. Then, in section 4.3 we discuss the kinematical reconstruction of the LSP mass. Schematically, the procedure is as follows:

$$E_{\text{jet}} \text{ distribution } \rightarrow E_\tau \rightarrow m_X. \tag{4.10}$$
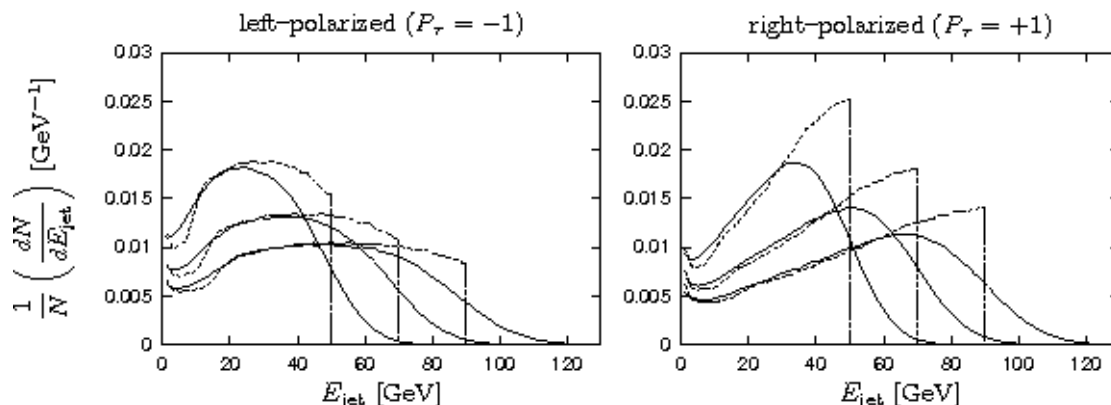
Figure 8: Tau jet energy distributions for left-polarized (left) and right-polarized (right) tau generated by TAUOLA. The primary tau energy is $E_\tau = 50, 70, 90\,\text{GeV}$ from left to right. The dashed lines show the spectrum without energy resolution effect, and the solid lines show the spectrum with detector energy resolution $\Delta E_\text{jet}/E_\text{jet} = 150\%/\sqrt{E_\text{jet}/\text{GeV}}$.

When $\tilde{\tau}$ decays into τ and invisible particle X, the tau energy E_τ is monochromatic (see eq. (4.2)). E_τ can be obtained by fitting the τ jet energy distribution :

$$\frac{dN}{dE_\text{jet}}(E_\text{jet};\ E_\tau) \qquad \text{where } E_\text{jet} \ = \ \sum_{i\,\neq\,\nu,\,\mu}^{\text{decay products}} E_i \ . \qquad (4.11)$$

Among the decay products of the τ lepton we omit the neutrinos and muons. In order to see the prospects of E_τ measurement with a finite number of events, we generate the events from τ decay by using the TAUOLA [26], and we perform a maximum-likelihood fitting of low statistics ("experimental") event sets by high statistics ("theoretical") distributions.

In practice, the observed jet energy distribution depends not only on the E_τ, but also on the detector resolution ΔE_jet and the tau polarization P_τ:

$$\frac{dN}{dE_\text{jet}}(E_\text{jet};\ E_\tau, P_\tau, \Delta E_\text{jet}). \qquad (4.12)$$

To obtain theoretical predictions for $dN/dE_\text{jet}(E_\text{jet};\ E_\tau, P_\tau, \Delta E_\text{jet})$, we have generated tau decay events with high statistics run of TAUOLA for the parameter space $E_\tau = 30$ — $125\,\text{GeV}$ and $-1 \leq P_\tau \leq 1$, while fixing $\Delta E_\text{jet}/E_\text{jet} = 150\% /\sqrt{E_\text{jet}/\text{GeV}}$.[4] For each single τ decay generated by TAUOLA, the jet energy E_jet is calculated, and then smeared by a Gaussian fluctuation with a variance $\sigma^2 = (\Delta E_\text{jet})^2$. Fig 8 shows examples of the jet energy distribution.

In order to see a realistic situation, we generate a small number of tau lepton decays for a fixed parameter set of $(E_\tau,\ P_\tau,\ \Delta E_\text{jet})$, and then fit the result by the "theoretical"

---

[4]We have generated 10^6 events for each of the parameter sets $E_\tau = 30, 31, 32, \ldots 109, 125\,\text{GeV}$ and $P_\tau = \pm 1$ (i.e., 96×2 parameter sets $\times 10^6$ events), and interpolated the distribution between those parameter points.
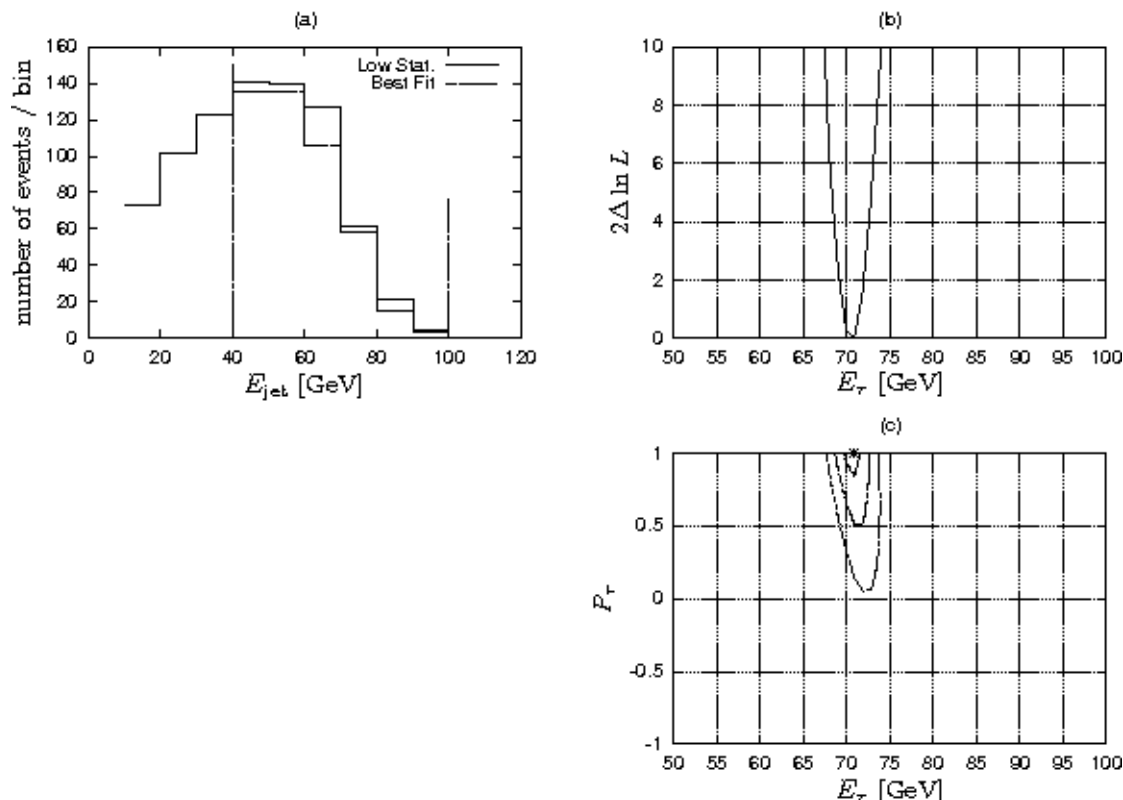
Figure 9: An example of maximum-likelihood fit of low statistics events from tau decays. (a) Energy distribution of tau jet events generated from 1000 decaying tau leptons for $E_\tau = 70\,\mathrm{GeV}$, $\Delta E_{\mathrm{jet}}/E_{\mathrm{jet}} = 150\%/\sqrt{E_{\mathrm{jet}}/\mathrm{GeV}}$ and $P_\tau = +0.8$ (solid histogram), and the best fit distribution (dotted histogram). Only the bins between the vertical lines are used for the fit (see text). (b) $2\Delta \ln L = 2(\ln L_{\max} - \ln L)$ projected onto the E_τ axis. (c) Contour plots of $2\Delta \ln L = 1, 4, 9$ projected onto the (P_τ, E_τ) plane.

distribution obtained above. Here and hereafter, we assume that the energy resolution will be known in advance. Examples are shown in figure 9 and figure 10 for total number of decaying tau leptons $N_\tau = 1000$ and $N_\tau = 100$, respectively. The energy of τ jets which are not contained in the detector may not be measured precisely. The N_τ corresponds to the number of well contained events. Some comments are in order here. (i) We take 1 bin $= 10\,\mathrm{GeV}$. (ii) For the maximum-likelihood fitting we take only the bins with number of events ≥ 1, and the bins above the peak energy, which in the examples of figure 9(a) and 10(a) correspond to the bins between the two vertical lines. (iii) We then calculate the $\ln L$ distribution in the parameter space of (E_τ, P_τ) as follows

$$\ln L(E_\tau, P_\tau) = \sum_{i=\mathrm{bins}} \ln f_{\mathrm{P}}\left(N_i^{\mathrm{low}}; N_i^{\mathrm{high}}(E_\tau, P_\tau)\right) \tag{4.13}$$

where $f_{\mathrm{P}}(n;\nu) = \nu^n e^{-\nu}/n!$ is the Poisson distribution, N_i^{low} is the number of events in the i-th bin for the low statistics run, and $N_i^{\mathrm{high}}(E_\tau, P_\tau)$ is the predicted number of events in
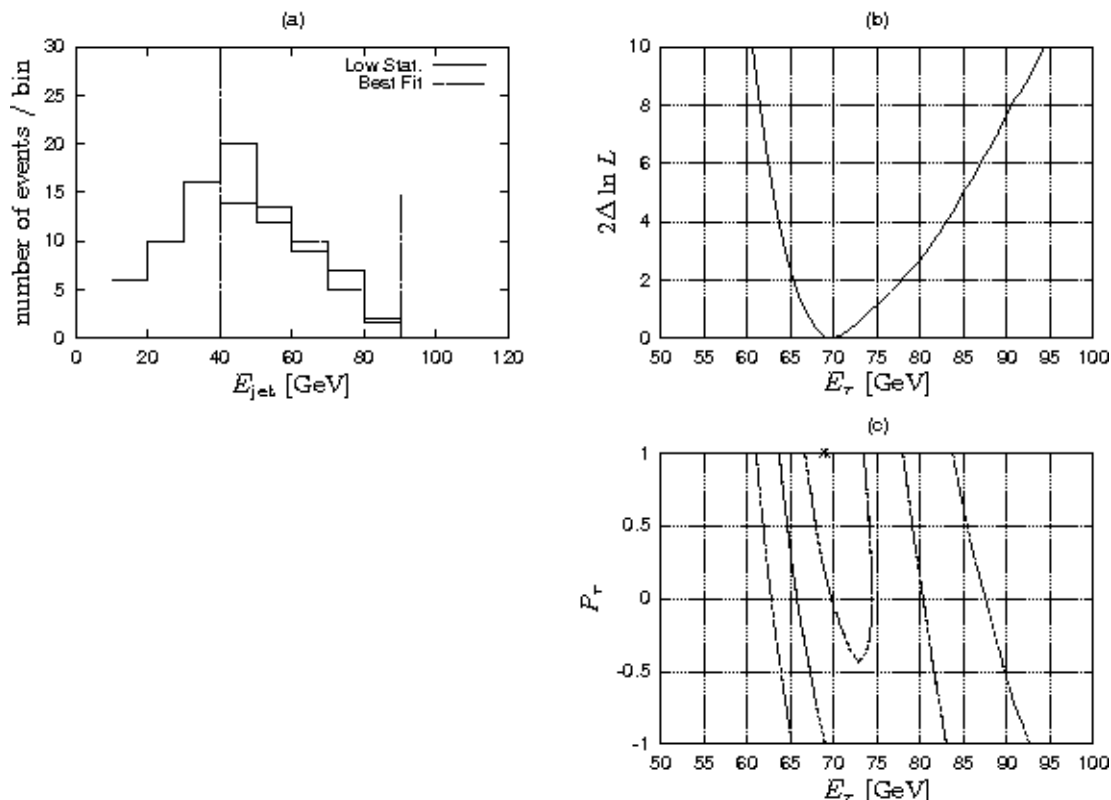
Figure 10: An example of maximum-likelihood fit of low statistics events from tau decays. The same as figure 9 but with 100 decaying tau leptons.

the i-th bin as a function of the parameter set (E_τ, P_τ), normalized by the total number of decaying tau leptons. Here, we assume that the total number of stopped $\tilde{\tau}$ is known, i.e., the total number of events is *not* taken as a free parameter for the fit.

The $n\sigma$ confidence interval can be estimated by the range $2\Delta \ln L = 2(\ln L_{\max} - \ln L) \leq n^2$ projected onto the E_τ axis [see figures 9(b) and 10(b)]. One can see that the primary tau energy can be determined within an error of a few GeV. From figure 9(c) one can also see that the polarization is hardly determined by the energy distribution analysis even with $N_\tau = 1000$. This is because the sensitivity to the polarization becomes very weak once the finite detector resolution is taken into account (cf. figure 8).

To estimate the statistical error in E_τ measurement we have generated the event sets with same statistics $N_\tau = 100$ (1000) and repeat the fit on E_τ and P_τ to obtain the best fit value of the E_τ, E_τ^{best}. In figure 11, we show the distribution of E_τ^{best} for $E_\tau = 50, 70, 90 \,\mathrm{GeV}$, $P_\tau = 1$, and $\Delta E_{\mathrm{jet}}/E_{\mathrm{jet}} = 150\%/\sqrt{E/\mathrm{GeV}}$. From the variances of these distributions, we estimate the 1σ uncertainty of E_τ as

$$\delta E_\tau/E_\tau = 61\%/\sqrt{E_\tau/\mathrm{GeV}} \qquad \text{for} \quad N = 100 \,, \tag{4.14}$$

$$\delta E_\tau/E_\tau = 15\%/\sqrt{E_\tau/\mathrm{GeV}} \qquad \text{for} \quad N = 1000 \,. \tag{4.15}$$
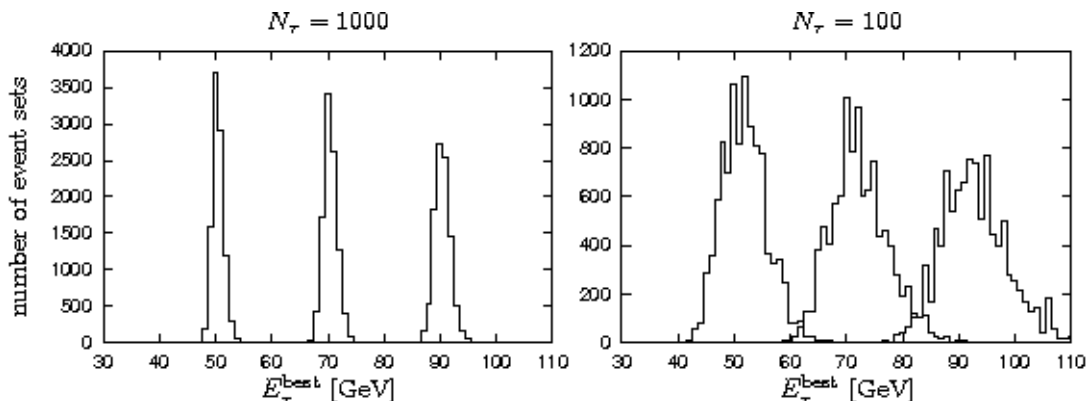
Figure 11: Distribution of $E_\tau^{\rm best}$ for $E_\tau = 50, 70$ and $90\,{\rm GeV}$ (from left to the right), for $N_\tau = 1000$ (left) and $N_\tau = 100$ (right).

4.3 Determination of the LSP mass

Now we can estimate the uncertainty of the LSP mass. In figure 12 we plot the range of reconstructed LSP mass

$$\widehat{m_X} = \sqrt{\widehat{m_{\tilde\tau}}^2 + m_\tau^2 - 2\widehat{m_{\tilde\tau}}\widehat{E_\tau}} \,, \tag{4.16}$$

where

$$E_\tau - \delta E_\tau(E_\tau) \ \leq \ \widehat{E_\tau} \ \leq \ E_\tau + \delta E_\tau(E_\tau) \tag{4.17}$$

and $E_\tau = (m_{\tilde\tau}^2 + m_\tau^2 - m_X^2)/2m_{\tilde\tau}$. Note that the reconstructed LSP mass depends on not only E_τ but also the measured CNLSP mass $\widehat{m_{\tilde\tau}}$. In figure 12 we show the range of LSP mass for $\widehat{m_{\tilde\tau}} = m_{\tilde\tau}$ (solid lines) and $0.99m_{\tilde\tau} \leq \widehat{m_{\tilde\tau}} \leq 1.01m_{\tilde\tau}$ (dashed lines), the latter corresponding to 1% uncertainty of the CNLSP mass. The stau mass determination from time of flight was discussed in [1, 27, 4]. For CMS detector the mass resolution is estimated as 10-20% in each event and less than 1% for ~ 1000 events.

As can be seen in figure 12, the kinematical reconstruction of the LSP mass is possible if m_X is sufficiently large, $m_X \gtrsim 0.15m_{\tilde\tau}$ for $N_{\tilde\tau} = 1000$ and $m_X \gtrsim 0.25m_{\tilde\tau}$ for $N_{\tilde\tau} = 100$. Otherwise one can get only an upper bound on the mass m_X.

4.4 Measurement of the "Planck scale"

Finally, if the LSP is the gravitino ($X = \tilde{G}$), the uncertainty of the reconstructed gravitino mass $\widehat{m_{\tilde{G}}}$ translates into an uncertainty of the supergravity Planck scale, which is obtained by substituting $\widehat{m_{\tilde{G}}}$ for $m_{\tilde{G}}$ in eq. (4.4). To take into account the error of $m_{\tilde\tau}$, we also substitute $\widehat{m_{\tilde\tau}}$ for $m_{\tilde\tau}$. Eq. (4.4) then becomes

$$\widehat{M_{\rm pl}}^2 = \frac{1}{3\pi\Gamma_{\tilde\tau}} \frac{\left(\widehat{m_{\tilde\tau}}\widehat{E_\tau} - m_\tau^2\right)\left(\widehat{E_\tau}^2 - m_\tau^2\right)^{3/2}}{\widehat{m_{\tilde\tau}}^2 + m_\tau^2 - 2\widehat{m_{\tilde\tau}}\widehat{E_\tau}} \,, \tag{4.18}$$
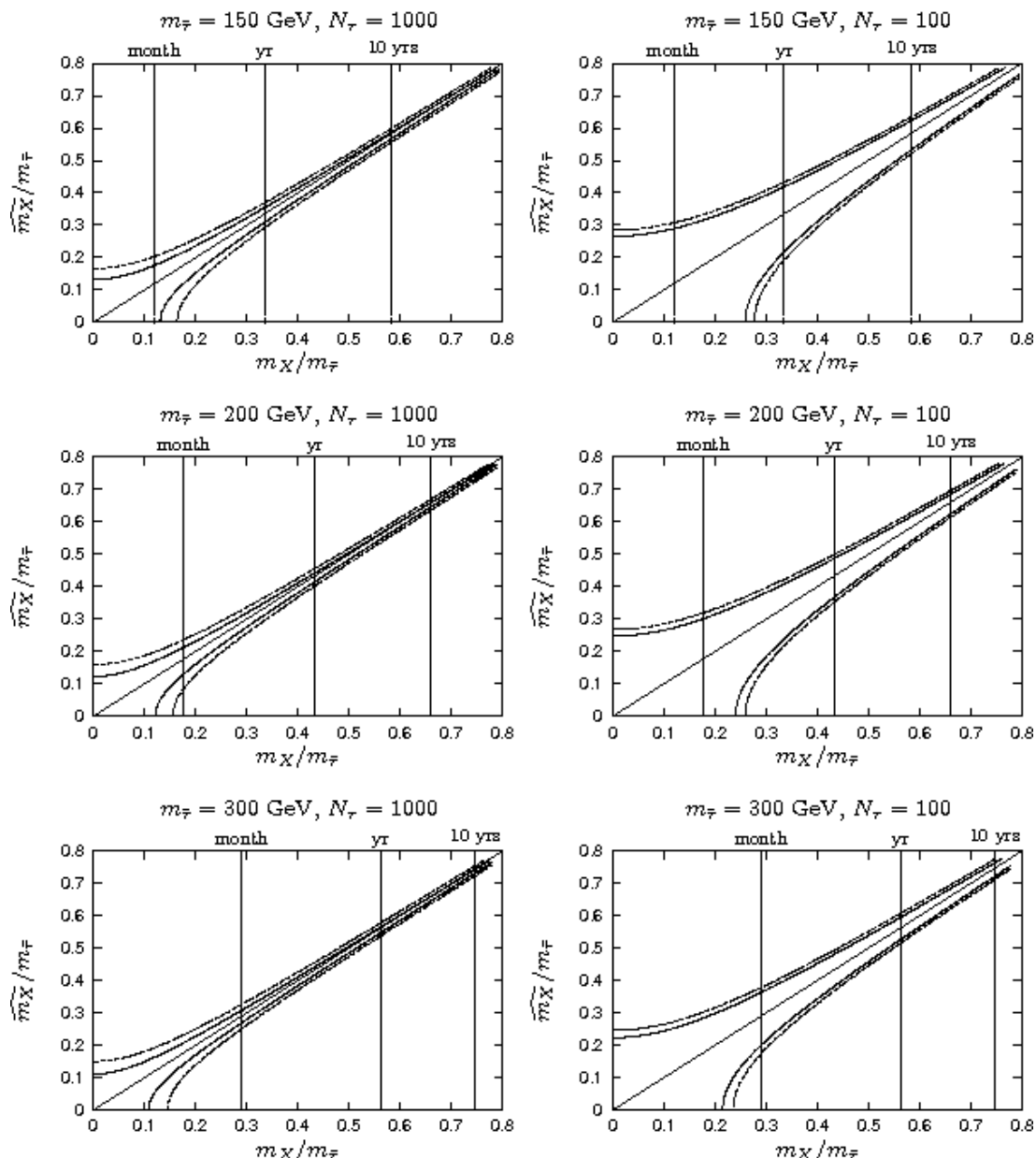
Figure 12: Uncertainty of the reconstructed LSP mass, corresponding to the estimated 1σ uncertainty of E_τ, for $N_\tau = 1000$ and 100, and $m_{\tilde\tau} = 150, 200$ and $300\,\text{GeV}$. Solid lines represent the case without an error of $m_{\tilde\tau}$, and dashed lines include 1% uncertainty of $m_{\tilde\tau}$. Vertical dotted lines represent the stau lifetime of 1 month, 1 year, and 10 years in the case of gravitino LSP $(X = \tilde{G})$.

which is shown in figure 13 for $\widehat{m_{\tilde\tau}} = m_{\tilde\tau}$ (solid lines) and $0.99 m_{\tilde\tau} \leq \widehat{m_{\tilde\tau}} \leq 1.01 m_{\tilde\tau}$ (dashed lines). Here we do not include the uncertainty of the lifetime measurement, which simply affects the measured Planck scale as $M_{\text{pl}} \propto (1/\Gamma_{\tilde\tau})^{1/2}$. Neglecting the τ-lepton mass,
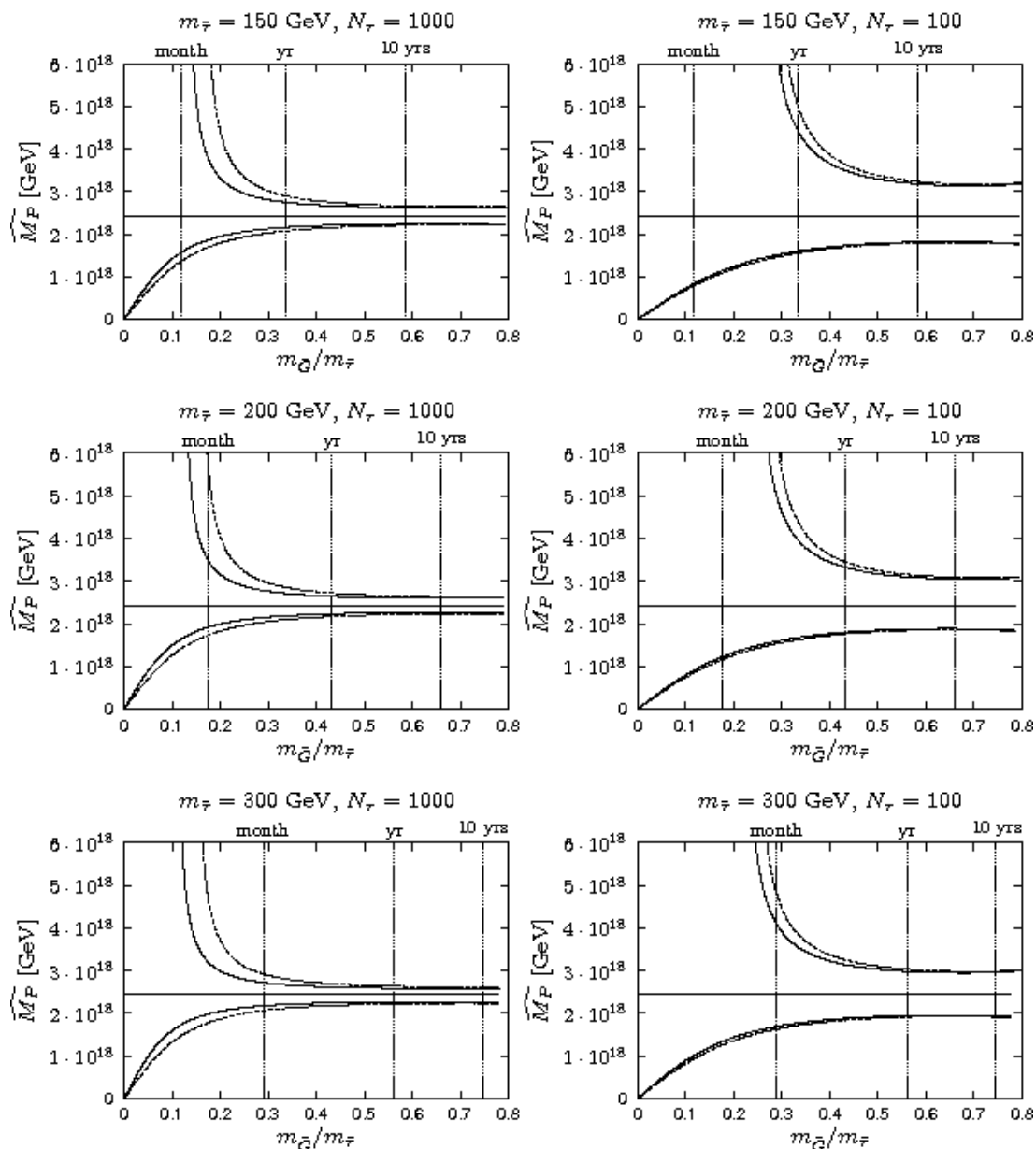
Figure 13: Uncertainty of the Planck scale measurement, corresponding to the estimated 1σ uncertainty of E_τ, for $N_\tau = 1000$ and 100, and $m_{\tilde\tau} = 150$, 200, and $300\,\mathrm{GeV}$. Solid lines represent the case without an error of $m_{\tilde\tau}$ measurement, and dashed lines include 1% uncertainty of $m_{\tilde\tau}$. Vertical dotted lines represent the stau lifetime of 1 month, 1 year, and 10 years.

eq. (4.18) is simplified as

$$\widehat{M_{\mathrm{pl}}}^2 \simeq \frac{1}{3\pi\Gamma_{\tilde\tau}} \frac{\widehat{E_\tau}^4}{\widehat{m_{\tilde\tau}} - 2\widehat{E_\tau}} \,. \tag{4.19}$$

As discussed in the previous section, the kinematical reconstruction of the gravitino mass is possible only if $m_{\tilde G}$ is sufficiently large, $m_{\tilde G} \gtrsim 0.15 m_{\tilde\tau}$ for $N_{\tilde\tau} = 1000$ and $m_{\tilde G} \gtrsim$

$0.25 m_{\tilde{\tau}}$ for $N_{\tilde{\tau}} = 100$. For smaller values of the gravitino mass, one can get only a lower bound on the Planck scale $M_{\rm pl}$.

One can see whether the determined 'Planck scale' is inconsistent with the Planck scale of the Einstein gravity, $M_{\rm pl} = 2.4 \times 10^{18}$ GeV. In other words, one can test the assumption of the decay $\tilde{\tau} \to \tau \tilde{G}$ by comparing the observed lifetime with the predicted lifetime. For example, if the NLSP dominantly decays into axino, the lifetime would be far shorter compared with gravitino assumption for a fixed mass m_X, leading to a smaller value of fitted $M_{\rm pl}$. Suppose for instance one measures $m_{\tilde{\tau}} = 150$ GeV and $m_X = 30$ GeV. When $X = \tilde{a}$, the lifetime becomes $\mathcal{O}(10 \text{ sec})$ for $f_a \simeq 10^{11}$ GeV and $m_{\tilde{B}} \simeq m_{\tilde{\tau}}$ [cf. eq. (4.8)]. If one uses eq. (4.18), a "Planck scale" $\widehat{M_{\rm pl}} = \mathcal{O}(10^{15} \text{ GeV})$ would be obtained, thereby falsifying the gravitino assumption.

4.5 Model points and cosmological constraints

We now discuss mSUGRA model points discussed in section 3, together with cosmological constraints. In the early universe, the $\tilde{\tau}$ CNLSP has been in thermal equilibrium until its decoupling, $T_d \sim 0.04 m_{\tilde{\tau}}$. If such a particle has a very long lifetime, as discussed in this paper, its decay during or after the big-bang nucleosynthesis (BBN), $T_{\rm BBN} \sim 1$ MeV, may spoil the successful prediction of BBN [28, 29]. In the models with $\tilde{\tau}$ NLSP and $\tilde{G}$ LSP, this leads to severe constraints on the parameter space of $(m_{\tilde{\tau}}, m_{\tilde{G}})$, in particular to upper bounds on the gravitino mass for a given stau mass [30, 31].

Furthermore, it has been recently pointed out that a heavy charged particle can form a bound state with light elements during the BBN, which can lead to new effects and/or severer constraints [32]. In this paper we do not discuss these effects because it is difficult to evaluate the net effect quantitatively and it still awaits detailed analysis.

We should also mention that those BBN constraints may disappear if there is entropy production between the stau decoupling ($T_d \sim m_{\tilde{\tau}}/20$) and the BBN ($T_{\rm BBN} \sim 1$ MeV), because the stau abundance is diluted before its decay [33].

Keeping in mind the possibilities of severer bounds and also a possible loophole, let us discuss the cases of $m_{\tilde{\tau}} = 150$ GeV and $m_{\tilde{\tau}} = 340$ GeV, corresponding to the mSUGRA model points ϵ and ζ. According to the latest analyses [31] including the effects of the hadronic decay [29], the bounds on the gravitino are $m_{\tilde{G}} \lesssim (20\text{--}80)$ GeV for $m_{\tilde{\tau}} \simeq 150$ GeV and $m_{\tilde{G}} \lesssim (40\text{--}200)$ GeV for $m_{\tilde{\tau}} \simeq 340$ GeV.[5] The ranges of upper bounds correspond to the uncertainties of various bounds from primordial light elements.

For $m_{\tilde{\tau}} = 150$ GeV (model point ϵ), as can be seen in table 1, one could collect more than 1000 staus for $300\,{\rm fb}^{-1}$. The bound $m_{\tilde{G}} \lesssim (20\text{--}80)$ GeV then suggests that the measurement of the gravitino mass and the "Planck scale" may become possible if one assumes conservative BBN bounds and if the gravitino mass is sufficiently large (cf. figures 12 and 13). For $m_{\tilde{\tau}} = 340$ GeV (model point ζ), the measurement would become easier if one could collect the same number of staus (cf. figures 12 and 13). However, from table 1 we find that expected number of stopped CNLSP is around 30 for $300\,{\rm fb}^{-1}$. This

---

[5]These constraints were derived without using the bound on the ^{3}He. If one adopts it, the constraints become severer (cf. [29]).

is because gluino mass is above $2\,\mathrm{TeV}$ for this point and production cross section is small. One needs SLHC ($\int \mathcal{L} = 1000\mathrm{fb}^{-1}$) to collect $\mathcal{O}(100)$ events.

In the case of axino LSP, the BBN bound is much weaker because the lifetime of the CNLSP stau becomes much shorter [see eq. (4.8)]. Hence, the axino mass measurement is plausible for sufficiently large $m_{\tilde{a}}/m_{\tilde{\tau}}$.

5. Light axino vs gravitino: the rare decay of the CNLSP

5.1 Low energy effective action of the axino and gravitino involving photon

When $m_{\tilde{G}} \lesssim 0.2 m_{\tilde{\tau}}$, it is difficult to determine the gravitino mass from τ energy measurement at stopper-detector. Axino is a motivated candidate which couples weakly to the MSSM particle with comparable strength to the gravitino. In this section we therefore compare the decay $\tilde{\tau} \to \tilde{a}\tau\gamma$ with the decay $\tilde{\tau} \to \tilde{G}\tau\gamma$. For simplicity, we will assume the NLSP is pure 'right-handed' stau, $\tilde{\tau} = \tilde{\tau}_R$ throughout this section. Extension to the case with mixing with $\tilde{\tau}_L$ is straightforward, and the mixing angle dependence is expected to be small.

The gravitino is a spin-3/2 particle. However, in the limit where $m_{\tilde{G}} \ll m_{\tilde{\tau}}$, the effective interaction to MSSM particles would be reduced to that of spin 1/2 particle, goldstino $\tilde{\chi}$. The effective action relevant to the $\tilde{\tau}_R$ decay is given as follows,

$$ L = \frac{m_{\tilde{\tau}}^2}{\sqrt{3}m_{\tilde{G}}M_{\mathrm{pl}}} (\bar{\tilde{\chi}}\tau_R \tilde{\tau}_R^* + H.c.) + \frac{-m_{\tilde{B}}}{4\sqrt{6}m_{3/2}M_{\mathrm{pl}}} \bar{\tilde{\chi}}[\gamma^\mu, \gamma^\nu]\tilde{B}(\cos\theta_W F_{\mu\nu} - \sin\theta_W Z_{\mu\nu}). \quad (5.1) $$

The action is similar to that of axino given in eqs. (4.5) and (4.6) except the coupling coefficients. The relative weight of the two terms in eq. (5.1) are fixed by the supergravity, while for the axino the coefficient in eq. (4.6) is induced from eq. (4.5) by the radiative corrections. Note that the term proportional to $X[\gamma^\mu, \gamma^\nu]\tilde{B}F_{\mu\nu}$ is a non renormalizable coupling of the photon to gravitino or axino and induces significantly different γ, τ distribution.

The axino three body decay $\tilde{\tau} \to \gamma\tau\tilde{a}$ proceeds through the diagrams shown in figure 14, where the hatched triangle express the effective vertex shown in eq. (4.6). On the other hand, the relevant diagrams for the three body decay into goldstino $\tilde{\tau} \to \gamma\tau\tilde{\chi}$, are given in figure 15. The diagram corresponding to the top right of figure 14 does not exist for the goldstino case. The difference of the actions and the relevant diagrams will appear as the deviation of the decay distributions. In the appendix, we list the three body decay differential width into gravitino/axino in the limit where the gravitino/axino mass can be neglected compared to $m_{\tilde{\tau}}$. The formula for the massive gravitino and axino are given in ref. [6].

5.2 Numerical results

The three body decay $\tilde{\tau} \to \tau\gamma X$ should be visible in the stopper-detector if it has an ability to measure charged tracks, and also segmented into small units. The position where $\tilde{\tau}$ decays in the detector is the position where the charged track by the π^+, μ and e from τ is initiated. For hadronic tau decays, a $\pi^\pm$ is always in the decay products, sometimes
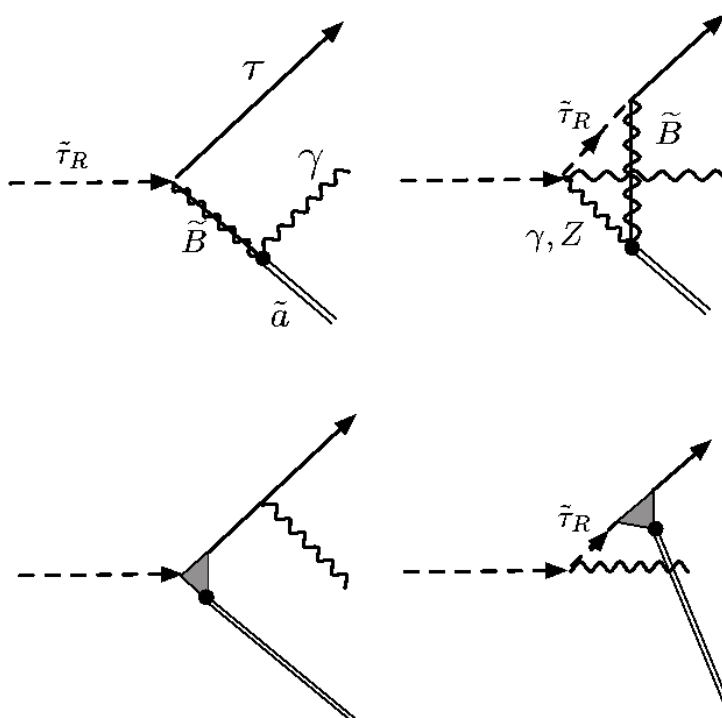
Figure 14: Leading Feynman diagrams for $\tilde{\tau} \to \tau\gamma\tilde{a}$.

with photons coming from π^0 decays. Photons are converted into electron after passing $\sim$ one radiation length X_0. Therefore for the iron based detector with $\rho = 5(2)\mathrm{g/cm^3}$, the photon shower starts 2.8(7)cm from the decay point. In summary, the three body decay of $\tilde{\tau} \to \tau\gamma X$ is identified as a charged track (which might be associated with collinear EM showers) + an isolated hard EM shower pointing back to the point where charged track is started. If the segmentation is not good enough, the efficiency to discriminate EM showers from $\pi^\pm$ would be reduced.

As can be seen in the appendix, the three body decay amplitude can be written as a function of the angle between photon and τ, θ, and E_γ. To be conservative we assume the energy resolution for the isolated photon shower is $\Delta E_\gamma/E_\gamma = 100\%/\sqrt{E_\gamma/\mathrm{GeV}}$ and ignore the angular resolution of the photon momentum. (In the following E_γ denotes the photon energy after taking into account of this finite resolution effect.) Note that the shortest length of the detector is 3.5 m, which corresponds to $1750\mathrm{g/cm^2}$ for $\rho = 5\mathrm{g/cm^3}$. The EM showers are likely contained in the stopper because we only need $200\mathrm{g/cm^2}$ to fully absorb them.

We need to require several cuts for the accepted events.

- Experimentally, the angle between τ and γ must be large enough to avoid the overlap between τ decay products and prompt γ. We only use the events where $\cos\theta < 0.866$. We do not lose sensitivity to the differece between the two decays $\tilde{\tau} \to \tau\gamma\tilde{a}/\tilde{G}$ by
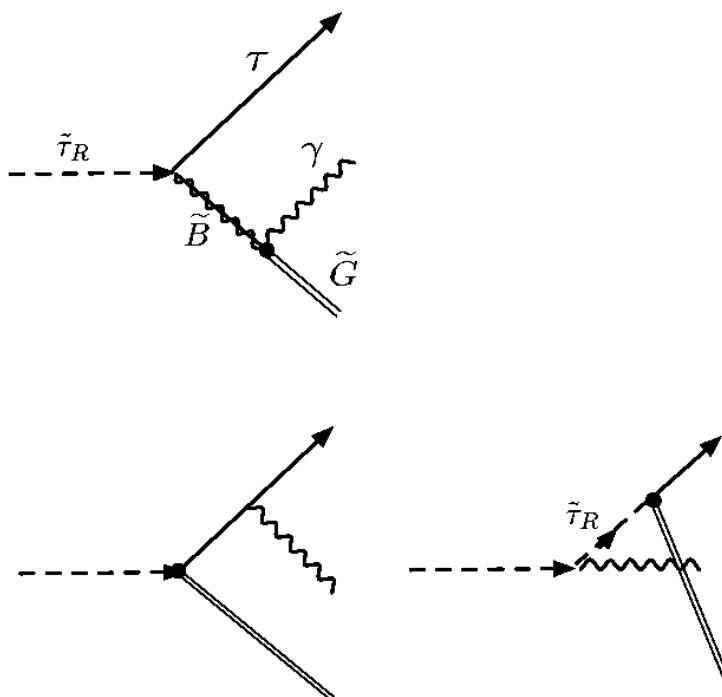
Figure 15: Feynman diagrams for $\tilde{\tau} \rightarrow \tau\gamma\tilde{G}$ in the goldstino limit.

cutting these events. In the collinear region, the amplitude is dominated by the contributions from QED vertex, which is common for both of the decays.

- The three body decay amplitude suffers soft and collinear singularity. Because we only adopt simple leading order calculation, we require $E_\gamma > 10\,\text{GeV}$ and $E_\tau > 10\,\text{GeV}$.

We define the ratio

$$R(X) = \Gamma(\tilde{\tau} \rightarrow X\gamma\tau)|_{\text{after cut}}/\Gamma(\tilde{\tau} \rightarrow X\tau) \tag{5.2}$$

The dependence of R on the MSSM parameter is quite different between $X = \tilde{a}$ and $X = \tilde{G}$. While $\tilde{\tau} \rightarrow \tilde{a}\tau$ is one loop process controlled by the parameter ξ, the three body decay contains a tree level contribution which depends on non-renormalizable axino-$\tilde{B}$-gauge coupling (top left of figure 14).

When ξ is small, the tree level contribution plays a dominant role in the three body decay into axino. This can be seen in figure 16, where the ratio $R(\tilde{a})$ is plotted as a function of the mass difference $m_{\tilde{B}} - m_{\tilde{\tau}}$. We also fix $m_X = 1\,\text{GeV}$ but $R(X)$ is insensitive to m_X. $R(\tilde{a})$ is enhanced when the mass difference between $m_{\tilde{B}}$ and $m_{\tilde{\tau}}$ is small relative to the $\tilde{\tau}$ mass. This is because the two body decay of axino is suppressed by $m_{\tilde{B}}^2$. The branching ratio ranges from 8% to 0.5% for the model parameters given in the figure. On the other hand, the branching ratio $Br(\tilde{\tau} \rightarrow \tau\gamma\tilde{G})$ is well below 1% for the parameter given in figure 16. $Br(\tilde{\tau} \rightarrow \tau\gamma\tilde{G})/Br(\tilde{\tau} \rightarrow \tau\tilde{G}) \sim 0.56\%$ (0.84%) for $m_{\tilde{\tau}} = 100(190)\,\text{GeV}$ respectively.
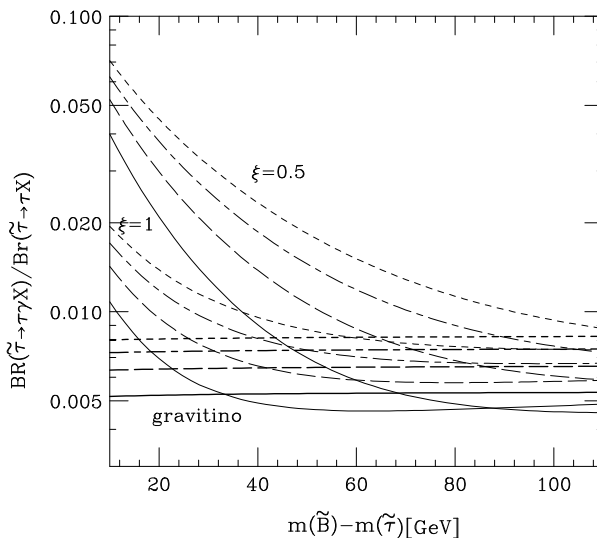
Figure 16: The ratio $R(X) = \Gamma(\tilde{\tau} \to X\gamma\tau)/\Gamma(\tilde{\tau} \to X\tau)$ as a function of $m_{\tilde{B}} - m_{\tilde{\tau}}$. The solid, dashed, dot-dashed, short-dashed curves correspond to the case where $m_{\tilde{\tau}} = 100, 130, 160, 190 \, \text{GeV}$ respectively. Lines which increase toward smaller mass difference corresponds to $X = \tilde{a}$. The $X = \tilde{G}$ lines do not show significant bino mass dependence.

When the three body decay branching ratio turns out be above 5%, 200 stopped $\tilde{\tau}$ is enough to see the 3 σ deviation from the gravitino assumption. We estimate the number of events N_{event} stopped in the detector, which is required to find 3σ deviation from the gravitino scenario as follows;

$$N_{\text{event}} \frac{(Br(\tilde{\tau} \to \tau\gamma\tilde{a}) - Br(\tilde{\tau} \to \tau\gamma\tilde{G}))^2}{Br(\tilde{\tau} \to \tau\gamma\tilde{a})} = 9. \tag{5.3}$$

The N_{event} as a function of $m_{\tilde{B}} - m_{\tilde{\tau}}$ is given in figure 17. Each curve increases as $m_{\tilde{B}} - m_{\tilde{\tau}}$ is increased up to the value where $Br(\tilde{\tau} \to \tau\gamma\tilde{a})$ coincides with $Br(\tilde{\tau} \to \tau\gamma\tilde{G})$. When $m_{\tilde{B}} - m_{\tilde{\tau}} < 20 \, \text{GeV}$, $\mathcal{O}(1000)$ ($\mathcal{O}(10000)$) stopped $\tilde{\tau}$ are enough to see the deviation from the measurement of R for $\xi = 0.5(1)$ respectively.

Not only the branching ratio, but also the decay distribution contain the information of the invisible particle. The axino decay distribution can be enhanced at the region where $x_\gamma = 2E_\gamma/m_{\tilde{\tau}}$ is large and $\cos\theta$ is small, namely hard photon and τ is back to back [6]. This occurs when ξ is small and relative importance of the direct axino-bino-gauge boson coupling is enhanced.

In figure 18, left panel shows the E_γ distribution for different $\cos\theta$ intervals. Here we fix $\xi = 1$, $m_{\tilde{B}} = 130$ GeV, and $m_{\tilde{\tau}} = 100 \, \text{GeV}$. The distribution has significantly hard component for $\cos\theta < 0$ when compared with that of gravitino in the right panel. The enhancement of back-to-back events is a signature of an axino, and clear τ and γ separation is not required to distinguish them.

We now estimate the the number of CNLSP decays in the stopper to see the 3 σ deviation between $\tilde{\tau} \to \tilde{a}\gamma\tau$ and $\tilde{G}\gamma\tau$ from the decay distribution. We define $\Delta\chi^2$ like

– 25 –
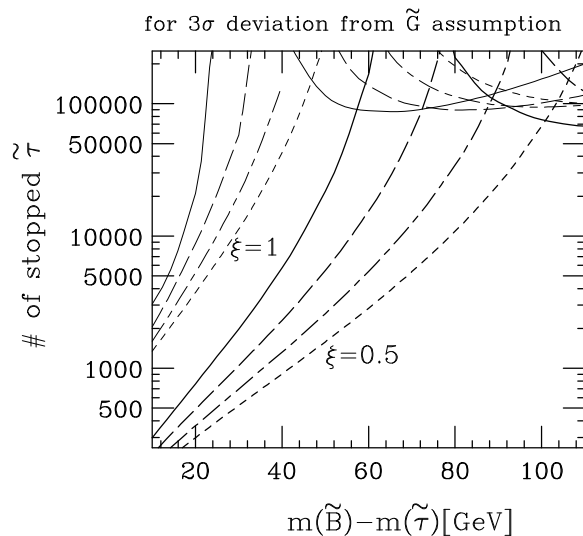
Figure 17: The statistics required to find the branching ratio $R(\tilde{a}) = \Gamma(\tilde{\tau} \to \tau\gamma\tilde{a})/\Gamma(\tilde{\tau} \to \tau\tilde{a})$ deviates more than 3 sigma from the prediction for $R(\tilde{G})$. The lines corresponds to different stau mass as in figure 16.
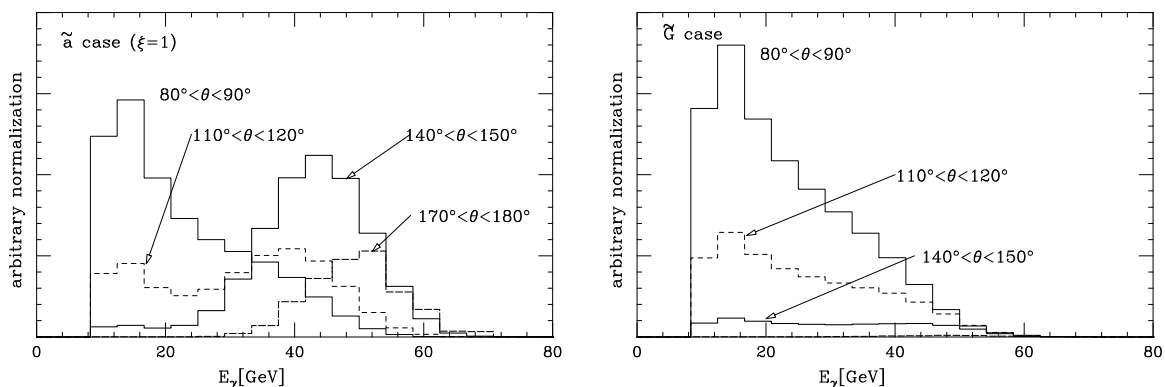

Figure 18: The distribution of E_γ in some θ intervals for $\tilde{\tau} \to \tau\gamma X$ decay. left panel: $X = \tilde{a}$ ($\xi = 1$), right panel: $X = \tilde{G}$. $m_{\tilde{\tau}} = 100\,\text{GeV}$, and $m_{\tilde{B}} = 130\,\text{GeV}$.

function from the differential decay width;

$$\Delta\chi^2_{\text{dist}}(m_{\tilde{\tau}}, m_X, m_{\tilde{B}}, \xi, \Delta E_\gamma, \Delta\theta) = \Sigma_i \frac{(n_i(\tilde{a}) - \bar{n}_i(\tilde{G}))^2}{n_i(\tilde{a})}. \tag{5.4}$$

Here, $n_i(\tilde{a})$ is the number of event in a i-th bin for $\tilde{\tau} \to \tau\gamma\tilde{a}$ when the number of stopped $\tilde{\tau}$ is $N_{\text{gen}} = 10^5$. ΔE_γ and $\Delta\theta$ is the bin size in E_γ and θ. We divide the E_γ and θ into 8 bins and 3 bins respectively, for the range $0 < E_\gamma < m_{\tilde{\tau}}$ and $0 < \theta < \pi$;

$$\Delta E = m_{\tilde{\tau}}/8, \quad \Delta\theta = \pi/3. \tag{5.5}$$

The photon energy resolution of the detector is assumed $\Delta E_\gamma/E_\gamma = 100\%/\sqrt{E_\gamma/\text{GeV}}$. We apply the cut $\cos\theta < 0.866$, $E_\gamma > 10\,\text{GeV}$ and $E_\tau > 10\,\text{GeV}$. On the other hand, $\bar{n}_i(\tilde{G})$ is
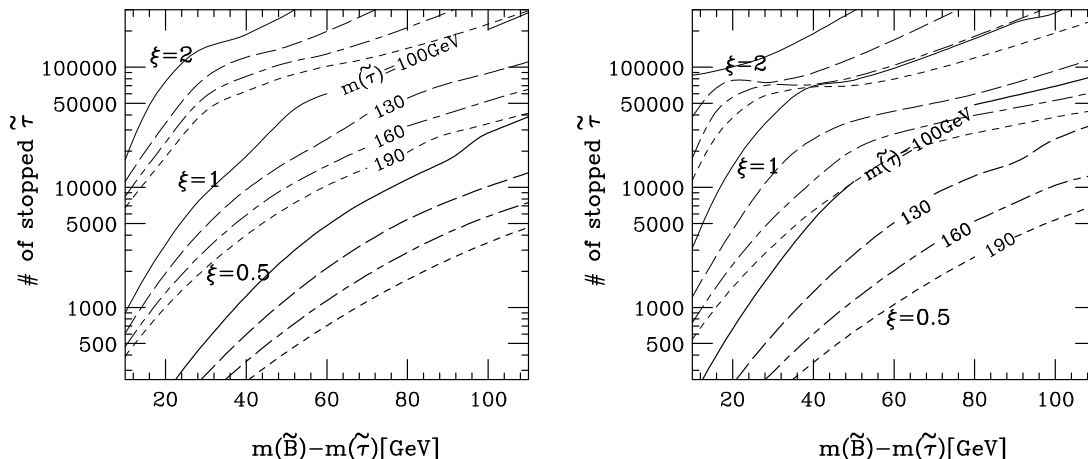
Figure 19: Statistics required to distinguish axino scenario from gravitino scenario. left for $m_{\tilde{G}} = m_{\tilde{a}} = 1\,\text{GeV}$ and right for $m_{\tilde{G}} = m_{\tilde{a}} = 30\,\text{GeV}$

the number of event in a i-th bin for $\tilde{\tau} \to \tau\gamma\tilde{G}$ with $m_{\tilde{G}} = m_{\tilde{a}}$ normalized so that the total number is same to that of axino three body decay. Namely, we do not use the information for $R(x)$ in our fit.

From $\Delta\chi^2_{\text{dist}}$, we define $N_{\text{dist}}(3\sigma)$, the number of stopped $\tilde{\tau}$ required to see the 3σ deviation between $\tilde{\tau} \to \tau\gamma\tilde{a}$ and $\tilde{\tau} \to \tau\gamma\tilde{G}$ as follows,

$$N_{\text{dist}}(3\sigma) = N_{\text{gen}}/(\Delta\chi^2_{\text{dist}}/9). \tag{5.6}$$

We show the $N_{\text{dist}}(\sigma)$ as a function of $m_{\tilde{B}} - m_{\tilde{\tau}}$ in figure 19. The sensitivity is significantly increased from the estimate using the branching ratio only. For $m_{\tilde{B}} - m_{\tilde{\tau}} = 40\,\text{GeV}$, the deviation may be visible for $\mathcal{O}(1000)$ events for $\xi = 0.5$ ($\mathcal{O}(10000)$ events for $\xi = 1$).

Finally, we estimate sensitivity at our model points in section 3. For simplicity we assume $\tilde{\tau} = \tilde{\tau}_R$. In general $\tilde{\tau}_R$ is mixed with $\tilde{\tau}_L$. The mixing angle is defined as

$$\tilde{\tau}_1 = \tilde{\tau}_L \cos\theta_{\tilde{\tau}} + \tilde{\tau}_R \sin\theta_{\tilde{\tau}} . \tag{5.7}$$

For model points discussed in table 2, the angle is $\sin\theta_{\tilde{\tau}} \sim 0.9$. The effect of the mixing angle in the axino decay is small because the amplitude of τ_L is suppressed by both by the small $\cos^2\theta_{\tilde{\tau}}$ factor and smaller hypercharge, and can be safely ignored.

In figure 20 the expected sensitivity at the stopper-detector is shown. Here, long-dashed (long-short-dashed, dashed) line corresponds to the required statistics for $\xi = 0.5$ (0.75, 1) for different Λ, while the upper and lower solid lines correspond to the number of stopped CNLSP for $300\,\text{fb}^{-1}$ and $3000\,\text{fb}^{-1}$. One can address the difference between axino and gravitino for $\Lambda \sim 55(65)\text{TeV}$ or less for $\mathcal{L} = 3000\,\text{fb}^{-1}$ and $\xi = 1$ (0.75). Note that the expected reach in Λ is essentially determined by the SUSY production cross section, as they decrease steeply with increasing Λ. We therefore show the gluino masses scale on the top of the figure.
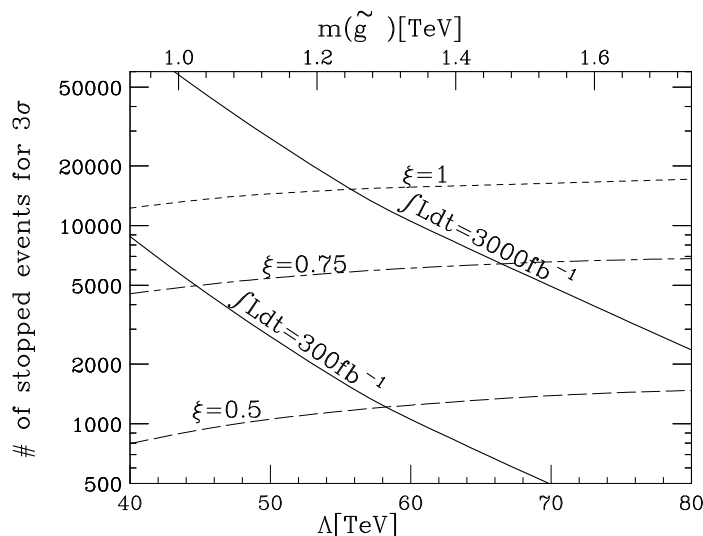
Figure 20: Solid lines are the expected number of stopped events for $300(3000)\text{fb}^{-1}$ luminosity for GM points with $40\text{TeV} < \Lambda < 80\text{TeV}$. Dashed lines are number of required stopped events to see 3-σ deviation in the $E_\gamma - \cos\theta$ distribution of $\tilde\tau \to \tau\gamma\tilde{a}$ from those expected for the decay $\tilde\tau \to \tau\gamma\tilde{G}$.

6. Discussion

In this paper we investigate the physics of the long-lived charged next lightest SUSY particle (CNLSP), which may be explored at a massive stopper-detector placed next to the CMS detector at the LHC. We assume the CNLSP is the lighter scalar tau, $\tilde\tau$, which decay into τX where X is a invisible particle. A natural candidate of the particle X is a gravitino but we also consider the case where X is axino $\tilde{a}$.

In this paper, we assume very large stopper-detector next to the CMS detector, with total mass of 8 kton. The stopper must have a capability to measure the position where the CNLSP stopped, and also the energy of the τ decay products. If the detector can be highly segmented, it is also possible to identify the τ decay products separately. The number of stopped NLSP ranges from $\mathcal{O}(10^4)$ to $\mathcal{O}(100)$ for gluino and squark with mass below $2\,\text{TeV}$. If the size of the detector should be smaller, the number of the events must be scaled down linearly.

We estimate the statistical error for E_τ, which can be determined from the end point of the tau jet energy. We assume that the energy resolution of the detector is $150\%/\sqrt{E/\text{GeV}}$. $\delta E_\tau/E_\tau \simeq 60\%/\sqrt{E_\tau/\text{GeV}}$ ($15\%/\sqrt{E_\tau/\text{GeV}}$) can be achieved for the statistics of the order of $N_{\text{stopped}} = 100(1000)$. When LSP mass is above $0.2m_{\tilde\tau}$, one can constrain the gravitino mass both from above and below. From the lifetime and gravitino mass measurement, the supergravity Planck scale M_{pl} can be measured. If many CNLSP can be accumulated, one can even study the three body decay of the CNLP $\tilde\tau \to \tau\gamma X$. When the dominant decay mode of the $\tilde\tau$ is $\tilde\tau \to \tilde{a}\tau$, we may be able to see the deviation of the decay branching ratio and the distribution from the $X = \tilde{G}$ case.

Finally we comment on the strategy to proceed this experiment. SUSY particles will

be found in the early stage of the LHC experiment if SUSY scale is $\mathcal{O}(1\text{ TeV})$. If LSP is gravitino or axino and the NLSP is charged and long-lived, it would also be recognized easily. The detector proposed in this paper may be placed after the existence of long-lived CNLSP is observed, roughly at the same time to the high luminosity run of the LHC, or the proposed super LHC run.

It should also be noted that, although we have concentrated on SUSY models with gravitino (axino) LSP and stau NLSP, the stopper-detector proposed in this paper would be useful if any kind of long-lived particle which is electrically charged and/or colored will be found at the LHC. (See e.g., [34] for a recent review on (meta)-stable massive particles at colliders.) Such particles will eventually decay because they cannot be completely stable from cosmological considerations. Thus, the lifetime measurement and the study of the decay products will become a primary physics goal in any case, and a stopper-detector can play a crucial role for it.

LHC experiment has a great potential to explore new physics in TeV regions. It is important to explore new possibilities that can be done with LHC. In this paper we have proposed a large additional detector in the CMS cavern when the long-lived CNLSP is found. This requires a significant modification of the CMS experiment. The reward is low systematics study of the CNLSP decay which primarily serve for the study of the gravitino sector. The determination of gravitino mass either from the lifetime or (independently) from E_τ measurement would give us a direct information of the total SUSY breaking scale. Together with high precision determination of the MSSM sector expected with the CNSLP momentum information, the nature of the interaction of the MSSM sector and hidden sector can be studied in detail. We hope this paper is useful for further, and more realistic studies.

Acknowledgments

A. The three body decay of stau

In this appendix we list the differential decay width of $\tilde{\tau}_R$ decay into $\gamma\tau X$ where X is either gravitino or axino in limit where $m_X \ll m_{\tilde{\tau}_R}$. Formulas in this appendix are obtained by taking massless limits $m_{\tilde{G}}/m_{\tilde{a}} \to 0$ of the formulas in ref. [6]. The $\tilde{\tau}_R$ decay width to $\tau\gamma\tilde{G}$ is given as follows;

$$\frac{d^2\Gamma(\tilde{\tau}_R \to \tau\gamma\tilde{G})}{dx_\gamma d\cos\theta} = \frac{m_{\tilde{\tau}}}{512\pi^3} \frac{x_\gamma(1-x_\gamma)}{[1-(x_\gamma/2)(1-\cos\theta)]^2} \sum_{\text{spins}} |\mathcal{M}(\tilde{\tau}_R \to \tau\gamma\tilde{G})|^2 \qquad (A.1)$$

where

$$\sum_{\text{spins}} |M(\tilde{\tau}_R \to \tau\gamma\tilde{G})|^2 = \frac{8\pi\alpha}{3} \frac{m_{\tilde{\tau}}^2}{M_{\text{pl}}^2 A_{\tilde{G}}} F_{\text{diff}}^{\tilde{G}}(x_\gamma, \cos\theta, A_{\tilde{B}}). \qquad (A.2)$$

and

$$F_{\text{diff}}^{\tilde{G}} = \frac{1+\cos\theta}{1-\cos\theta}\left[-x_\gamma + \frac{2}{x_\gamma^2} + \frac{1}{1-x_\gamma}\right.$$
$$\left. +1 + \frac{4x_\gamma - 2(1-\cos\theta) - 4}{2 - x_\gamma(1-\cos\theta)} + \frac{4 - 4x_\gamma}{\{2 - x_\gamma(1-\cos\theta)\}^2}\right]$$
$$+\frac{1-x_\gamma}{2 - x_\gamma(1-\cos\theta)}\left(-4 + 2x - \frac{4}{x_\gamma}\right) + \frac{4(1-x_\gamma)^2}{\{2 - x_\gamma(1-\cos\theta)\}^2}$$
$$+\frac{1}{\{x_\gamma(1+\cos\theta) - 2A_{\tilde{B}} + A_{\tilde{B}}x_\gamma(1-\cos\theta)\}^2} \times$$
$$\times\left[2A_{\tilde{B}}^2(1-x_\gamma)\left\{x_\gamma^2 - 2x_\gamma + \frac{4}{x_\gamma} - (x_\gamma^2 - 2x_\gamma - 2)\cos\theta\right\}\right.$$
$$+A_{\tilde{B}}(1+\cos\theta)(4 - 3x_\gamma + x_\gamma\cos\theta)(x_\gamma^2 - x_\gamma - 2)$$
$$\left.-(1+\cos\theta)^2 x_\gamma(x_\gamma^2 - x_\gamma - 2)\right]. \tag{A.3}$$

Here

$$x_\gamma = 2E_\gamma/m_{\tilde{\tau}}, \quad A_{\tilde{B}} = (m_{\tilde{B}}/m_{\tilde{\tau}})^2, A_{\tilde{G}} = (m_{\tilde{G}}/m_{\tilde{\tau}})^2, \tag{A.4}$$

and θ is the angle between τ and γ.

For the case of massless axino, we find

$$\frac{d^2\Gamma(\tilde{\tau}_R \to \tau\gamma\tilde{a})}{dx_\gamma d\cos\theta} = \frac{m_{\tilde{\tau}}}{512\pi^3}\frac{x_\gamma(1-x_\gamma)}{[1 - (x_\gamma/2)(1-\cos\theta)]^2}\sum_{\text{spins}}|\mathcal{M}(\tilde{\tau}_R \to \tau\gamma\tilde{a})|^2, \tag{A.5}$$

where

$$\sum_{\text{spins}}|M(\tilde{\tau}_R \to \tau\gamma\tilde{a})|^2 = \frac{\alpha^3 C_{\tilde{a}YY}^2}{\pi\cos^4\theta_W}\frac{m_{\tilde{\tau}}^2}{f_a^2}F_{\text{diff}}^{\tilde{a}}(x_\gamma, \cos\theta, A_{\tilde{B}}), \tag{A.6}$$

$$F_{\text{diff}}^{\tilde{a}}(x_\gamma, \cos\theta, A_{\tilde{B}}) = \frac{x_\gamma^2(1-x_\gamma)(1+\cos\theta)\{1 + \cos\theta + A_{\tilde{B}}(1-\cos\theta)\}}{\{x_\gamma(1+\cos\theta) - 2A_{\tilde{B}} + A_{\tilde{B}}x_\gamma(1-\cos\theta)\}^2}$$
$$+A\frac{A_{\tilde{B}}(1+\cos\theta)}{x_\gamma(1+\cos\theta) - 2A_{\tilde{B}} + A_{\tilde{B}}x_\gamma(1-\cos\theta)}$$
$$+\frac{1}{4}A^2\frac{1+\cos\theta}{1-\cos\theta}A_{\tilde{B}}\left(\frac{1}{1-x_\gamma} + \frac{2}{x_\gamma^2}\right), \tag{A.7}$$

$$A = \frac{3\alpha}{\pi\cos^2\theta_W}\xi\log\left(\frac{f_a}{m}\right). \tag{A.8}$$

References

[1] ATLAS, *Detector and physics performance*, Technical Design Report, vol II CERN/LHCC/99-15.

[2] K. Hamaguchi, Y. Kuno, T. Nakaya and M.M. Nojiri, *A study of late decaying charged particles at future colliders*, Phys. Rev. **D 70** (2004) 115007 [hep-ph/0409248].

[3] J.L. Feng and B.T. Smith, *Slepton trapping at the large hadron and international linear colliders*, *Phys. Rev.* **D 71** (2005) 015004 [hep-ph/0409278].

[4] A. De Roeck et al., *Supersymmetric benchmarks with non-universal scalar masses or gravitino dark matter*, hep-ph/0508198.

[5] W. Buchmuller, K. Hamaguchi, M. Ratz and T. Yanagida, *Supergravity at colliders*, *Phys. Lett.* **B 588** (2004) 90 [hep-ph/0402179]; *Gravitino and goldstino at colliders*, hep-ph/0403203.

[6] A. Brandenburg, L. Covi, K. Hamaguchi, L. Roszkowski and F.D. Steffen, *Signatures of axinos and gravitinos at colliders*, *Phys. Lett.* **B 617** (2005) 99 [hep-ph/0501287].

[7] CMS technical proposal, CERN/LHCC/94-38 (1994).

[8] ATLAS technical proposal CERN/LHCC/94-43 (1994).

[9] S.Grohmann, CERN, ST-CV, *Concepts of refrigeration circuit design for CMS tracker cooling*, at the homepage of TS/CV/DC section of CERN.

[10] PARTICLE DATA GROUP collaboration, S. Eidelman et al., *Review of particle physics*, *Phys. Lett.* **B 592** (2004) 1.

[11] R.K. Bock, T. Hansl-Kozanecka and T.P. Shah, *Parametrization of the longitudinal development of hadronic showers in sampling calorimeters*, *Nucl. Instrum. Meth.* **186** (1981) 533.

[12] SOUDAN-2 collaboration, W.W.M. Allison et al., *The Soudan 2 detector: the design and construction of the tracking calorimeter modules*, *Nucl. Instrum. Meth.* **A 376** (1996) 36.

[13] H.U. Martyn, *Detecting metastable staus and gravitinos at the ILC*, *Eur. Phys. J.* **C 48** (2006) 15 [hep-ph/0605257].

[14] D.E. Kaplan, G.D. Kribs and M. Schmaltz, *Supersymmetry breaking through transparent extra dimensions*, *Phys. Rev.* **D 62** (2000) 035010 [hep-ph/9911293]; Z. Chacko, M.A. Luty, A.E. Nelson and E. Ponton, *Gaugino mediated supersymmetry breaking*, *JHEP* **01** (2000) 003 [hep-ph/9911323].

[15] W. Buchmuller, K. Hamaguchi and J. Kersten, *The gravitino in gaugino mediation*, *Phys. Lett.* **B 632** (2006) 366 [hep-ph/0506105].

[16] G.F. Giudice and R. Rattazzi, *Theories with gauge-mediated supersymmetry breaking*, *Phys. Rept.* **322** (1999) 419 [hep-ph/9801271].

[17] G. Corcella et al., *Herwig 6: an event generator for hadron emission reactions with interfering gluons (including supersymmetric processes)*, *JHEP* **01** (2001) 010 [hep-ph/0011363].

[18] H. Baer, F.E. Paige, S.D. Protopopescu and X. Tata, *Isajet 7.48: a Monte Carlo event generator for p p, p̄p and e⁺e⁻ reactions*, hep-ph/0001086.

[19] See http://www.hep.phy.cam.ac.uk/r̃ichardn/HERWIG/ISAWIG.

[20] M.J. Berger, J.S. Coursey and M.A. Zucker CRU report No.49.

[21] J.E. Kim, *Weak interaction singlet and strong CP invariance*, *Phys. Rev. Lett.* **43** (1979) 103; M.A. Shifman, A.I. Vainshtein and V.I. Zakharov, *Can confinement ensure natural CP invariance of strong interactions?*, *Nucl. Phys.* **B 166** (1980) 493.

[22] R.D. Peccei and H.R. Quinn, *CP conservation in the presence of instantons*, *Phys. Rev. Lett.* **38** (1977) 1440; *Constraints imposed by CP conservation in the presence of instantons*, *Phys. Rev.* **D 16** (1977) 1791.

[23] T. Goto and M. Yamaguchi, *Is axino dark matter possible in supergravity?*, *Phys. Lett.* **B 276** (1992) 103;
E.J. Chun, J.E. Kim and H.P. Nilles, *Axino mass*, *Phys. Lett.* **B 287** (1992) 123 [hep-ph/9205229];
E.J. Chun and A. Lukas, *Axino mass in supergravity models*, *Phys. Lett.* **B 357** (1995) 43 [hep-ph/9503233] and references therein.

[24] S. Schilling, F.D. Steffen, and D. Wyler, private communication.

[25] L. Covi, L. Roszkowski and M. Small, *Effects of squark processes on the axino CDM abundance*, *JHEP* **07** (2002) 023 [hep-ph/0206119].

[26] S. Jadach, J.H. Kuhn and Z. Was, *TAUOLA: a library of Monte Carlo programs to simulate decays of polarized tau leptons*, *Comput. Phys. Commun.* **64** (1990) 275;
M. Jezabek, Z. Was, S. Jadach and J.H. Kuhn, *The tau decay library TAUOLA, update with exact $O(\alpha)$ QED corrections in $\tau \to \mu$. (e) neutrino anti-neutrino decay modes*, *Comput. Phys. Commun.* **70** (1992) 69;
S. Jadach, Z. Was, R. Decker and J.H. Kuhn, *The tau decay library TAUOLA: version 2.4*, *Comput. Phys. Commun.* **76** (1993) 361.

[27] I. Hinchliffe and F.E. Paige, *Measurements in gauge mediated SUSY breaking models at LHC*, *Phys. Rev.* **D 60** (1999) 095002 [hep-ph/9812233].

[28] I.V. Falomkin et al., *Low-energy anti-p He-4 annihilation and problems of the modern cosmology, GUT and SUSY models*, *Nuovo Cim.* **A79** (1984) 193;
M.Y. Khlopov and A.D. Linde, *Is it easy to save the gravitino?*, *Phys. Lett.* **B 138** (1984) 265;
J.R. Ellis, J.E. Kim and D.V. Nanopoulos, *Cosmological gravitino regeneration and decay*, *Phys. Lett.* **B 145** (1984) 181.

[29] M. Kawasaki, K. Kohri and T. Moroi, *Big-bang nucleosynthesis and hadronic decay of long-lived massive particles*, *Phys. Rev.* **D 71** (2005) 083502 [astro-ph/0408426];
K. Jedamzik, *Big bang nucleosynthesis constraints on hadronically and electromagnetically decaying relic neutral particles*, *Phys. Rev.* **D 74** (2006) 103509 [hep-ph/0604251].

[30] T. Asaka, K. Hamaguchi and K. Suzuki, *Cosmological gravitino problem in gauge mediated supersymmetry breaking models*, *Phys. Lett.* **B 490** (2000) 136 [hep-ph/0005136];
M. Fujii, M. Ibe and T. Yanagida, *Upper bound on gluino mass from thermal leptogenesis*, *Phys. Lett.* **B 579** (2004) 6 [hep-ph/0310142].

[31] J.L. Feng, S. Su and F. Takayama, *Supergravity with a gravitino LSP*, *Phys. Rev.* **D 70** (2004) 075019 [hep-ph/0404231];
F.D. Steffen, *Gravitino dark matter and cosmological constraints*, *JCAP* **09** (2006) 001 [hep-ph/0605306].

[32] M. Pospelov, *Particle physics catalysis of thermal big bang nucleosynthesis*, hep-ph/0605215;
K. Kohri and F. Takayama, *Big bang nucleosynthesis with long lived charged massive particles*, hep-ph/0605243;
M. Kaplinghat and A. Rajaraman, *Big bang nucleosynthesis with bound states of long-lived charged particles*, *Phys. Rev.* **D 74** (2006) 103004 [astro-ph/0606209];

R.H. Cyburt, J. Ellis, B.D. Fields, K.A. Olive and V.C. Spanos, *Bound-state effects on light-element abundances in gravitino dark matter scenarios*, *JCAP* **11** (2006) 014 [astro-ph/0608562].

[33] W. Buchmuller, K. Hamaguchi, M. Ibe and T.T. Yanagida, *Eluding the BBN constraints on the stable gravitino*, hep-ph/0605164.

[34] M. Fairbairn et al., *Stable massive particles at colliders*, *Phys. Rept.* **438** (2007) 1 [hep-ph/0611040].